Synthesis and characterization of ordered mesoporous carbon

Efforts to induce graphite and N-Fe doped materials

Joel Hagman

A master thesis performed at:

Department of Chemical and Biological Engineering
Division of Applied Surface Chemistry
CHALMERS UNIVERSITY OF TECHNOLOGY
Göteborg, Sweden August 30, 2007

Supervisors:	Lic.Eng. Kjell Wikander, Applied Surface Chemistry
	Assistant Professor Anders Palmquist, Competence Centre for Catalysis and Applied Surface Chemistry
Examiniator:	Professor Krister Holmberg, Applied Surface Chemistry

Synthesis and characterization of ordered mesoporous carbon
Efforts to induce graphite and N-Fe doped materials
JOEL H. HAGMAN

© JOEL H. HAGMAN, 2007.

Department of Chemical and Biological Engineering
Division of Applied Surface Chemistry
Chalmers University of Technology
SE-412 96 Göteborg
Sweden
Telephone + 46 (0)31-772 1000

Printed by Chalmers Reproservice
Göteborg, Sweden 2007

Abstract

In this thesis, eleven mesoporous carbon materials have been synthesized and characterized via an templatory method from an ordered mesoporous silica as template. This silica template were synthesized and characterized as well. The characterization of the carbon materials have been made with respect to structural order, substances incorporated, specific surface, specific pore volume, pore volume distribution and pore diameter. The methods used to perform the characterisations have been N_2 physisorption, TEM, SEM-EDX, XPS, Raman, SAXS and WAXS. Some efforts have been made in order to dope the materials with N-Fe bonds as well as to induce graphitization.

During the synthesisation the different materials differs in the carbon precursor, iron source and temperature treatment. The carbon precursors used have been furfuryl alcohol (FA), furfuryl amine (FAm), pyrrole (Py) and acrylonitrile (AcN). The iron source used have been $FeCl_3$ dissolved in either paratoluene sulphone acid (PTSA), the carbon precursor or 1M HCl. The different temperature treatments have been made in such way that when the carbon precursor were to be pyrolysed, he material have been pyrolysed in either 800 °C or 1100 °C with N_2 as inert atmosphere. All materials except those made from acrylonitrile have been impregnated three times with carbon precursor and then pyrolysed three times. The N_2-physisorption of the acrylonitrile material showed that the pores of the silica template were totally filled with pyrolysed and polymerised carbon which made the material look finished and the silica removed after only on impregnation. unfortunately the pores must have collapsed or the carbon must have polymerised in the pore entrance since the amount of material after the removal of the silica were close to none. The other materials behaved normally and yielded approximately a 1:1 ratio between the amount of silica template used and the amount of carbon material achieved.

The result of the experiments showed that the order of the mesoporous carbon depends on the type of carbon precursor as well as how the iron source were presented into the pores. FAm with the $FeCl_3$ dissolved in the PTSA gave both a high Fe:N ratio and a clearly visible long range cubic ordered structure. The material were a bit more disordered if he $FeCl_3$ were dissolved in the FAm and there were no long range order if FAm were used without any $FeCl_3$. Using Py as carbon precursor gave the highest Fe:N ratio but the material were totally amorphous with respect to long range order. The acrylonitrile were hard to characterize since the amount of material were too little, but it appears to be difficult to dope the material with N and Fe and it seemed to lack long range order. The FA were used only as a reference and no $FeCl_3$ were added to this material. However, the long range order were clearly cubic. Compared to the FAm, which have a similar monomer structure, the FA did not seem to need an iron source to gain long range order.

All of the materials showed graphitic boundaries in both WAXS and Raman, but unfortunately there was impossible to measure the amount of these boundaries since the Raman results depended too much on where in the material the measurement were performed. Thus it is safest to say that the graphitization can be induced in pyrolysis at 800 °C but a higher temperature might give rise to more graphitization.

The XPS results were used both together with the SEM-EDX to show the content of the materials as well as the Fe:N ratios but might would have given an information whether the nitrogen and iron present in the material were bound as C-N-Fe. Unfortunately the XPS spectras were not resolved enough to be able to tell all peaks apart and it we not possible to say if such bonds existed.

Sammanfattning

I detta examensarbete har elva mesoporösa material framställts och karaktäriserats genom att använda ordnat mesoporöst kisel som mall. Kiselmallen har även den syntetiserats och karaktäriserats under projektets gång. Materialen har karaktäriserats med hänsyn till huruvida porerna erhållit kiselmallens ordning, vilka ämnen som kolet lyckats bli dopat med, specifik yta, specifik porvolym, porvolymsfördelning och pordiameter. De metoder som använts för karakterisering har varit N_2 fysisorption, TEM, SEM-EDX, XPS, Raman, SAXS och WAXS. Det har även gjorts försök att dopa kolmaterialet med N-Fe bindningar samt att få materialet grafitiskt.

Vid syntetiseringarna har de olika materialen framställts genom att variera kolkällan, hur järnet har introducerats in i porerna samt vid vilken temperatur materialen har pyrolyserats. Kolkällorna som använts har varit furfurylalkohol (FA), furfurylamin (FAm), pyrrol (Py) samt akrylonitril (AcN). Järnkällan har varit samma i alla försök men har varit löst i olika lösningsmedel, antingen i para-toluensulfonsyra (PTSA), i kolkällan eller i 1M HCl. Pyrolystemperaturerna som använts har antingen varit 800 °C eller 1100 °C med N_2 som inertatmosfär. Alla materialen, förutom de gjorda med akrylonitril impregnerades med kolkällan tre gånger och pyrolyserades tre gånger innan kiselmallen löstes upp med väteflourid. Att akrylonitril materialen inte fick samma behandling berodde på att N_2-fysisorptionen som gjordes mellan varje steg visade på att porerna var helt fyllda efter första pyrolysen. Då antagandet gjordes att materialet var färdigt löstes kiselmallen således upp efter bara en impregnering. Tyvärr visade det sig att materialen inte var helt färdiga, troligen hade porväggarna kollapsat eller så hade kolkällan reagerat i porernas ingång snarare än inuti porerna då mängden kolmaterial som var kvar efter kislets borttagande var försvinnande litet. De andra materialen betedde sig mera normalt och ungefär gick det att få ut 1:1 mellan mängden kiselmall satsat och mängden kolmaterial erhållen.

Resultaten av experimenten visar tydligt att ordningen på lång skala beror på kolkällan samt hur järnet introducerats in i porerna på kiselmallen. FAm med järnkloriden löst i PTSA gav både ett högt Fe:N ratio samt en tydlig kubisk ordning på porerna i kolmaterialet. Om järnkloriden istället löstes i FAm så minskade mängden både kväve och järn samt att porordningen blev otydligare. I det fallet då inget järn tillsattes när FAm användes som kolkälla så blev materialet amorft med avseende på porordningen. För materialet med Py som kolkälla så var Fe:N ration den klart högsta, men samtidigt så var materialets porer amorft ordnade. De akrylonitril baserade materialen var dock svåranalyserade då provmängderna var ytterst små. Det verkar som om att det var svårt att dopa kolet med N-Fe bindningar och materialet verkade bli amorft med hänsyn till porernas ordning. Furfurylalkohol användes bara som referensmaterial då denna saknar kvävegrupper, så inget järn tillsattes till detta material. Dock gick det att notera att materialets porer blev tydligt kubiskt ordnade trots avsaknaden av järnkälla, något som furfurylamin (som har nästan samma monomer) inte blev.

Alla materialen påvisade grafitiska områden i både WAXS och Raman. Dock gick det inte att bestämma halten av grafitiskt kol då Raman mätningarna var för beroende av var på materialet mätningen skedde. Det är därför säkrast att dra slutsatsen att grafitiska områden kan bildas vid pyrolys vid 800 °C men att högre temperatur eventuellt kan påverka storleken på dessa områden.

Både XPS och SEM-EDX användes för att bestämma halterna av ämnen i kolmaterialen samt således även Fe:N ration. Tanken var dock att XPS skulle kunna verifiera om det fanns C-N-Fe bindningar vilket tyvärr inte var möjligt. Då spektrana inte var upplösta nog för att med säkerhet kunna verifiera om bindningarna finns eller ej så får antagandet göras att de kan finnas men att ytterligare tester behövs för att verifiera eller vederlägga bindningarnas existens.

Contents

1 Background **1**
1.1 Fuel cells . . . 2
1.1.1 Basic principle of PEMFC . . . 2
1.1.2 Limitations of the fuel cell technology . . . 2
1.1.2.1 Catalyst . . . 3
1.1.2.2 Catalyst support . . . 3
1.1.2.3 Choice of catalyst . . . 3
1.2 Carbon as catalyst carrier . . . 4
1.2.1 Alternative catalyst materials . . . 4
1.3 Aim of this project . . . 4

2 Tools for nanomaterial synthesis **5**
2.1 Surfactants . . . 5
2.1.1 liquid crystals . . . 6
2.2 Mesoporous materials . . . 7

3 Experimental procedure **9**
3.1 Synthesis of ordered mesoporous silica . . . 9
3.2 Synthesis of ordered mesoporous carbon . . . 9
3.2.1 Furfuryl alcohol . . . 10
3.2.2 Furfuryl amine . . . 11
3.2.3 Pyrrole . . . 11
3.2.4 Acrylonitrile . . . 12
3.2.5 Pyrolysis temperature sequences . . . 12

4 Analytical Techniques **13**
4.1 N_2 physisorption . . . 13
4.2 Electron Microscopy . . . 14
4.2.1 SEM . . . 14
4.2.2 TEM . . . 15
4.3 Small and Wide Angle X-ray Scattering . . . 15
4.4 Raman . . . 16
4.5 X-ray Photoelectron Spectroscopy . . . 17

5 Results **19**
5.1 OMS . . . 19
5.2 Furfuryl alcohol . . . 20
5.3 Furfuryl amine . . . 23
5.4 Pyrrole . . . 28
5.5 Acrylonitrile . . . 32
5.6 Temperature treatment . . . 35
5.7 Deviations . . . 35

6 Conclusions **39**

7 Acknowledgements **41**

8 Appendix 1 **43**
8.1 N_2 physisorption data 43
8.2 SEM-EDX data 44
8.3 XPS data 44

1 Background

Fossil fuels are today used for a lot of everyday applications. Coke, oil and natural gas are used in powerplants to produce heat and electricity, people still use oil to heat their homes in oil furnaces and most of the vehicles are powered by gasoline and diesel. Even though the efficiency of the energy conversion is continuously increasing and the emission control programs makes the applications more environmental friendly, there are some issues with fossil fuel that need to be resolved. The energy consumption is constantly increasing which requires more energy and fuel to be produced. Since there is a limited amount of fossil fuel, continued use of petrol-based power is not a long term option. Even though there is a technical possibility to reduce the emission from fossil fuels, there will always be a release of otherwise stored carbon dioxide into the atmosphere, which may have a major impact on the climate. Due to the discharge of stored carbon dioxide (and other emissions) and the diminishing amount of fossil fuel, the only long term stable solution to the issue is to change to bio-renewable energy-carrying alternatives. One of the biggest areas to make changes in is fuels for vehicles since the transport sector is almost exclusively dependant on oil as energy carrier. Some of the options for alternate fuel are:

A. Biogas

B. Ethanol

C. Biodiesel

D. Electricity

Alternative A to C are all fuel types for combustion engines and can easily be obtained by modifying petrol engines (and there are already vehicles running on these kind of fuels). One problem with all combustion engines, however, is that there will always be some emissions of environmentally harmful substances. Especially nitrogen oxides, NO_x, emissions are hard to come by since most part of it is formed by the nitrogen present in the air inlet [4] and will be formed during combustion even if the fuel is nitrogen free. Aside from nitrogen oxides there are other environmentally harmful emissions such as sulphur oxides, SO_x, hydrocarbons, HC, and particular matter. These other emissions may be lowered (or removed completely) by altering or cleaning the fuel. To fully satisfy the issue of no emissions, the only alternative is to use electricity. There are tree ways to make use of electric power which are more or less emission free.

1. Batteries charged from the power grid in the city
2. Using solar panels on the car to directly transform solar energy into electricity
3. Fuel cells creating electricity from an on-board fuel

Option 1 exists today and is emission free if the electricity is produced by a non-pollution method[1]. The current drawback though is that the battery has a low capacity and requires long time to recharge. Also option 2 and 3 exists today, though mainly on a stage in development. Using solar panels usually generates insufficient amount of electricity to be a realistic alternative but is non-polluting provided a sustainable manufacturing of them. They also have the limitation of only producing electricity when exposed to the sun. Whether fuel cells are to be considered emission-free depends on the source of fuel used as well as the production of the fuel cell. There are some choices of hydrogen carriers such as pure hydrogen gas, alcohol, hydrogen stored in a metal-organic compound or metal hydrides and even oils (both bio-renewable and fossil[2]). Since there is no regular combustion in a fuel cell, a nitrogen free fuel will have no NO_x emissions (which combustion engines has). However, There will still be CO_2 emission if the hydrogen carrier is carbon based but since this will be from a bio-renewable source, the net emission is considered zero.

[1] It also depends on where the system boundaries are set, since the manufacture of the batteries may cause emissions

[2] Though using fossil fuel as hydrogen carrier wouldn't decrease our need for such limited resource

The H_2-powered fuel cell technology is a technology that will potentially meet the demands for a green. non-pollution energy conversion technique. There are several different types of fuel cells which differs in the working temperature, type of electrolyte and catalyst requirements. The Polymer electrolyte membrane fuel cell (PEFC or PEMFC) technique is considered as the most promising fuel cell for mobile applications, thanks to its high efficiency, fairly low operation temperature etc. The PEMFC is more closely described in section 1.1.1, though most fuel cells work in a similar way.

1.1 Fuel cells

As mentioned earlier, there are several different fuel cells. In this project only the PEMFC is taken in account since this work might give directions of how to further improve the PEMFC.

1.1.1 Basic principle of PEMFC

The hydrogen fuel enters at the anode side and is oxidized to protons and electrons. The protons travel to the cathode electrode through the proton conducting polymer membrane while the electrons must use the external circuit path via the electric engine of the vehicle. On the cathode side the protons, electrons and oxygen atoms meet each other and are reformed catalytically to water.

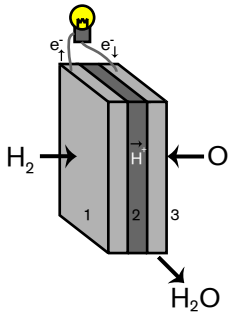

Figure 1.1: The PEM fuel cell with the H_2 entering at the anode (1), the proton transfer via the polymer membrane (2) and the oxygen entering at the anode (3) yielding water as the exhaust product

Pure hydrogen should preferably be used since it will not generate any other emission than water. However, due to low energy density and risk of explosion the hydrogen have to be stabilised in some other type of media. If the hydrogen carrier is an alcohol or other type of carbon based substance the carbon entering will be oxidised into carbon dioxide and thus a CO_2 emission will occur.

1.1.2 Limitations of the fuel cell technology

As briefly mentioned in section 1.1.1, one drawback is the low energy density of H_2. Since gasoline have a rather high energy density[3]compared to other fuels the biggest drawback of using other fuels will be the shorter operation range per refuelling, an issue that has to be solved.

[3]Gasoline have approximately 40 GJ m^{-3} while compressed hydrogen have approximately 10 GJ m^{-3} and ethanol have approximately 21.3 GJ m^{-3} [16]

1.1.2.1 Catalyst

The common catalyst used today in both cathode and anode electrodes is platinum. In the anode, supplied H_2will be oxidized into protons and electrons whereas O_2 will be reduced on the cathode and forms water together with the protons, transferred through the membrane, and electrons, which are transferred via the external circuit as current.

The activity of platinum for H_2 oxidation is very high and hence only a small amount of catalyst is necessary on the anode. The activity of platinum for the oxygen reduction is however relatively poor and hence a high catalyst loading is required.

Since the resources of platinum is very limited the availability is low and the price is therefore high. In order to commercialize the PEMFC to the public, the platinum dependency must be lowered. To address this issue research activities have been performed to investigate alloy catalyst in which the amount of platinum is significantly lowered thanks to the dilution with a transition metal. Platinum-transition metal (Pt-M) alloys that have been studied are e.g. Pt-Co, Pt-Fe, Pt-V, Pt-Ti, Pt-Ni etc. The activity of the oxygen reduction reaction of many Pt-M alloys has often been found higher than for pure platinum but they are limited by having a shorter life-time. Another research angle to address the issue has been to study oxides with low or even zero platinum content. Evaluation of the experiments have revealed observations of poor stability and a low activity [12]. The preparation methods is often ambitious, something that makes the catalyst expensive. Another approach is therefore to investigate low-cost catalysts. In such case can a low activity be compensated with a higher loading in the electrode. One such type of catalyst is the Fe-N-C family, first investigated by Dodelet et al [15].

1.1.2.2 Catalyst support

The catalyst support is used to keep the catalyst in the desired working area, i.e. where the reaction occurs. The common automotive car catalyst is attached to a monolith, which is placed in the exhaust piping underneath the car. The monolith structure is rather large and not applicable for a fuel cell application. The catalyst support in a PEMFC should be small enough to fit in the stack of fuel cells but porous enough to not reduce the mass flow and strong enough to keep the catalyst fixed. If porous carbon is used then the pores can be used for mass transport and the conducting properties of the carbon can transport the current generated. The drawback with porous carbon is that it is sensitive for oxidation and it is slowly decomposed if used for a longer period of time. Also, the pores of many carbon materials may have a mass transport limitations due to either being too small or being unevenly distributed. To avoid these problems ordered mesoporous carbon may be a solution. The mesopores are ordered and have a size between 2 to 50 nm, which potentially increases transport. To get a stronger structure, the carbon could be graphitizied since this brings short range order into the system that increases stability.

1.1.2.3 Choice of catalyst

One important bottleneck with current PEMFC catalysts is that platinum is almost the only element that is used. Due to the scarce supply and therefore high price of platinum this is an important problem to commercialize the PEMFC technology. Other metals with promising effects are palladium and ruthenium [2], which not are any good alternatives since they too are scarce. That is, using them instead will only lead to lowering the efficiency without increasing profit. The only real option is to use a catalyst with less efficiency that is based on materials with more abundant occurrence, since as long as the alternative is cheap enough it doesn't matter if ten times more are required to maintain the desired efficiency, it will still be more profitable then using precious metals. one such alternative is carbon with N-Fe bonds attached. Both nitrogen, iron and carbon are more common then platina and a lot cheaper.

1.2 Carbon as catalyst carrier

For efficient use of a catalyst it should be well dispersed in order to expose a large active surface area. In most applications he catalyst needs to be deposited onto a host material, a so-called support material, to be fixed at the reactor location. Carbon is often used in fuel cells thanks to its low weight, low price, high electric conductivity and relatively high surface area. Amorphous carbon is commonly used in fuel cells and Vulcan XC-72 is one such material. It consists of particles between 20-50 nm and has a specific surface area of approximately 230 m^2 g^{-1}. Thanks to the small particle diameter, deposited catalyst nanoparticles are able to be kept well-dispersed in the electrode. Nevertheless, it has been found that the long-term stability of catalyst loaded amorphus carbon in fuel cell electrodes is low since carbon is oxidized, probably catalysed by the deposited active catalyst. One effect of support decomposition is that the active catalyst migrates in the electrode. Loss of active surface area due to nanoparticle aggregation as well as membrane contamination are some negative effects. Carbon support materials with higher resistance towards oxidation is hence needed. This issue were mentioned in section 1.1.2.2 and as mentioned there, one solution to this might be graphitic carbon, which is much more stable and thus investigation of this is of interest.

1.2.1 Alternative catalyst materials

One benefit of using C-N-Fe as catalyst is the possibility to use ordered mesoporous carbon as support material. This makes the entire catalyst to act as a support material and removes (or at least lower) the need of extra support and thus lower the catalyst volume.

Another benefit is that if the entire structure have C-N-Fe bonds instead of only adding some to the surface is that there might be "self cleaning" properties induced. One problem with traditional catalysts is the loss of active material which leads to loss of efficiencyIf the entire structure is made with the same active properties, loss of active material will only open up for more surface with active sites.

1.3 Aim of this project

Since it is shown that Fe-N-C has activity for the oxygen reduction reaction, it is investigated if this kind of material is possible to prepare using a templatory method. The objective is to prepare ordered mesoporous carbon materials using different carbon, nitrogen and iron precursors and to investigate if such carbon materials, doped with N and Fe, can be synthesized. The materials will be characterized with respect to structural and compositional properties but also in order to find out whether a more graphite material can be obtained.

The effort to synthesize and characterise the different kind of OMC have been made in order to get an overview of what could be interesting to focus on in further analysis and further applications. Applications in which these materials may be used as catalyst and catalyst carriers for PEMFC.

2 Tools for nanomaterial synthesis

The theory for the creation of the nanomaterials produced during the project are presented in this chapter.

2.1 Surfactants

Molecules with a polar "head" and a non-polar "tail" usually tend to be attracted to surfaces while in solutions, thus the name surfactant.

Figure 2.1: Schematic of a surfactant showing the non-polar "tail" (1) and the polar "head" (2)

This surface attraction is caused by that only the part of the surfactant that matches the polarity of the solvent media will have favourable interactions with this medium. The insoluble part of the surfactant will have an unfavourable interaction with the solvent and is rejected. An interface is created when two medias are immiscible while in contact with each other. There are several different reasons why they are immiscible e.g. different chemical state[1], different viscosities or different polarity. Water, for example, is a polar solvent. In a water-surfactant system, the hydrophobic tail is drawn towards the water-air and water-vessel interfaces since the tail-air and the tail-vessel wall interactions are more favourable than the tail-water interaction [11].

When adding surfactants to a solution all surfaces will be covered immediately by the surfactant molecules. Not until the concentration of surfactants reaches the critical micelle formation concentration (CMC) will any free surfactant aggregation take form in the solution. What type of aggregation that is formed depends on

1. Type of system (water or oil as the continuous phase)
2. Type of surfactant
3. Surfactant concentration (above CMC)

Polymers can be used as surfactants by creating co-block polymers with different polarities of the blocks. One example of this is PE-PS block co-polymers that are used to mix polyethene with polystyrene, which normally are immiscible, in order to gain a material with properties from both polymers. An other example is Pluronic, which is a group of block co-polymers based on ethylene oxide and propylene oxide. The pluronic group is one of the many polymers that is commonly used as an surfactant and they can function as e.g. anti-foaming agents, wetting agents, dispersants, thickeners and emulsifiers.

If a block co-polymer is presented into a solution, it usually behaves like other surfactants and creates aggregations at concentrations $\geqslant$ CMC.

[1] E.g. solid, liquid or gaseous

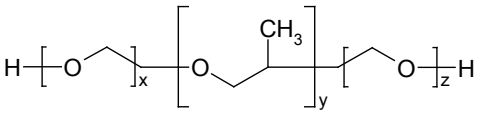

Figure 2.2: The chemical structure for P123

2.1.1 liquid crystals

When the concentration is above CMC, aggregation of the surfactant occurs. The first aggregation created is micelle formation, which are spheres with the hydrophobic tails inside the sphere away from the water and the hydrophilic heads out towards the water phase. The micelles does not have any order relative each other in the solution and move around randomly. When the concentration is increased further to be well above the CMC, the interaction forces between the micelles become important and the surfactant aggregations arrange themselves into ordered structures. In micelles start to grow forming other aggregation. The different aggregations gain order since the high concentration makes them unable to move around at random without interfering with each other. In figure 2.1.1 examples of surfactants at different concentrations are given.

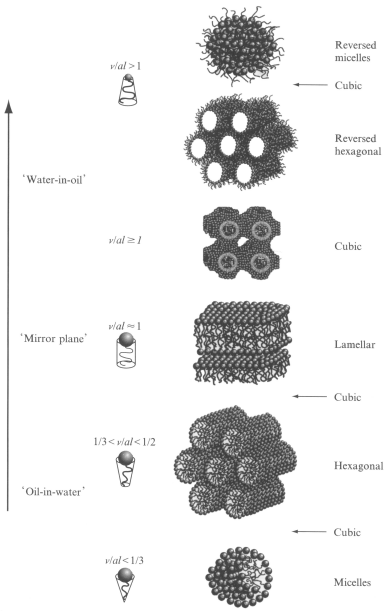

Figure 2.3: Schematic of typical surfactant aggregations at different concentrations. Image is reprinted from Holmberg et al. [11]

There are some different types of surfactants categorized by the of head: cationic, anionic, non ionic and zwitterionic (both anionic and cationic). Corresponding classification based on the tail group properties is: different chain length, multiple tails (i.e. gemini surfactant), spacer size for the gemini surfactant. The different head and tail group properties alter the properties of the surfactant e.g. what type of interfaces the surfactant prefers, temperature dependencies, CMC and solubility.

2.2 Mesoporous materials

Mesoporous materials have pores with a pore diameter between 2 to 50 nm. In 1992, it was first published synthesis methods of silica materials with ordered pore arrangement, so-called ordered mesoporous materials When the liquid crystal is impregnated with silica, the slurry is heat treated to make the silica stiffen after which the surfactants are washed away and remains are burned of. The silica have no formed to be a inverted template of the surfactant aggregation and since silica is rigid enough it's usable as a template to polymerise mesoporous carbon. The silica template is impregnated with a liquid carbon source, some catalyst or initiator and other substances that is desired in the finished product. The silica template will need to be impregnated in turns with pyrolysis in between in order to fill the pores entirely. The more the pores are filled, the more rigid will the final carbon material be since the carbon pores will be determined by the thickness of the silica walls and thus the carbon walls will be of the same size as the filled pores of the silica template (this is caused by that each time a casting is made of the previous template the new template will be inverted).

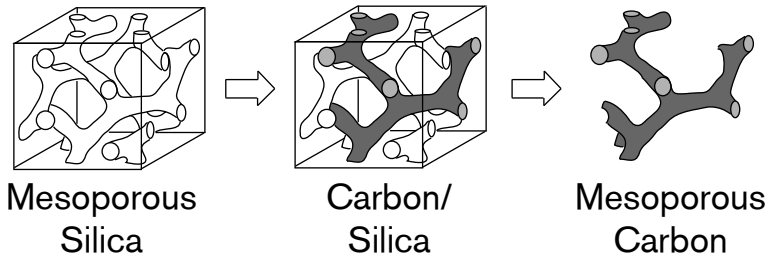

Figure 2.4: The general outline to create mesoporous carbon from a template is to: 1. Create the silica template from a silica source and surfactant system, 2. impregnate the silica pores with a carbon precursor, 3. Remove the silica structure (usually done with a strong acid e.g. HF)

When the pores of the silica template is filled, the silica template is removed by dissolving it in hydrofluoric acid which dissolves silica but not carbon. The finished carbon is then later washed and completed.

3 Experimental procedure

Below follows the experimental procedures for the materials prepared in this project.

3.1 Synthesis of ordered mesoporous silica

A silica template was created by mixing P123, TEOS, H_2O and HCl according to the method described by Kleitz et al in Chemical communications 2003 [13].
At first 20.3 g P123 (Aldrich, Mn 5800) were dissolved in 723.3 g water (MilliQ) and 39.4 g HCl (Riedel-de Haën, 37%) at 35 °C. When the P123 were entirely dissolved, 20.0 g butanol (Fluka, 98%) were added during continuous stirring for 1 hour after which 43- 2 g TEOS were added. Stirring continued for approximately 24 hours, still at 35 °C, before the mixture were put in oil bath for a hydrothermal treatment at 100 °C for 24 hours to mature. The silica template were vacuum filtrated and washed with ethanol (Aldrich, 95%) and MilliQ water. The silica was obtained as a white powder after calcination at 550 °C for 7 hours.

	Original Recipe	Scaled Recipe
P123 [g]	6.0	20.0
H_2O [g]	217.00	723.3
HCl [g]	11.8	39.3
Butanol [g]	6.0	20.0
TEOS [g]	12.9	43.0
Template Yield [g]	3.72 (theor)	12.4 (theor)
	11.80	11.85

Table 3.1: Formulation used when synthesising the ordered mesoporous silica

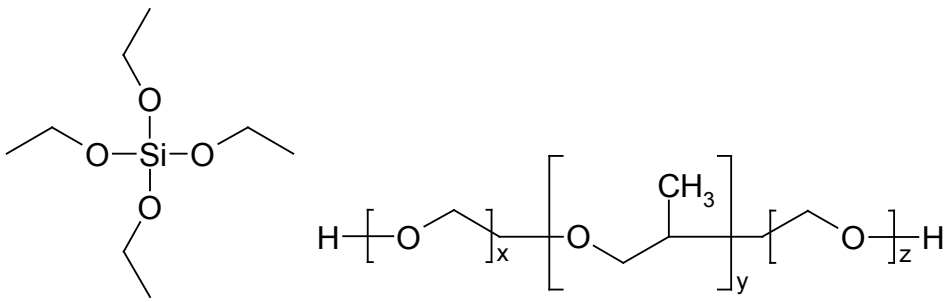

Figure 3.1: The chemical structure for TEOS and P123 respectively

3.2 Synthesis of ordered mesoporous carbon

There were seven different kind of carbon sources with variation of either the actual carbon source, how the iron were introduced into the template and different pre-treats. The different samples were named as Cx_1:Px_2 in order to tell them apart from the different carbon sources and the different pyrolysis stages.

Cx_1	Px_2
00 - Pure Furfuryl alcohol	0 - Impregnated once, no pyrolysis
01 - Furfuryl amine with $FeCl_3$ dissolved in catalyst	1 - Impregnated once, pyrolysed once
02 - Furfuryl amine with dissolved $FeCl_3$	2 - Impregnated twice, pyrolysed once
03 - Pure Furfuryl amine	3 - Impregnated twice, pyrolysed twice
04 - Pyrrole with $FeCl_3$ dissolved in 1M HCl as catalyst	4 - Impregnated trice, pyrolysed twice
05 - Acrylonitrile with $FeCl_3$ dissolved in 1M HCl	5 - Impregnated trice, pyrolysed trice
06 - Pre-treated Acrylonitrile with $FeCl_3$ dissolved in 1M HCl	6 - silica removed

Table 3.2: The translation of the sample names. Samples undertaking a high temperature treatment are denoted with CHx instead of C0x

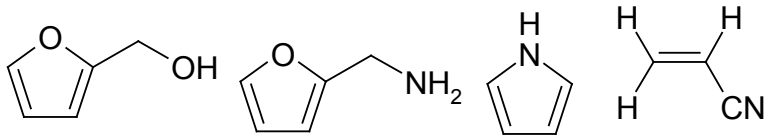

Figure 3.2: The chemical structure for furfuryl alcohol, furfuryl amine, pyrrole and acrylonitrile respectively

3.2.1 Furfuryl alcohol

This material will be referred to as C00:Px_2, in which x_2 will be replaced with the number that corresponds to the level of how complete the material is. See table 3.2 for full material nomenclature.
In order to have a pure carbon reference, the first sample produced had pure polyfurfurylic alcohol (FA) with p-toluene sulphonic acid (PTSA) as catalyst and no source of iron nor nitrogen. Using the method described by Fuertes et al. published in Microporous and mesoporous materials [7], the first material were synthesised.

2g of OMS were covered with 0.5M PTSA (Merck, >99%) in EtOH (Kemetyl, 99.5%) for 1 hour after which the silica were vacuum filtered and washed with alcohol. The silica is tried in a furnace at 80 °C for 2 hours followed by the pore impregnation of FA (Aldrich, 99%). The FA was added in such amount that matched the specific pore volume (measured with N_2 ads) and the silica were thoroughly mixed with a spatula. The impregnated sample were pyrolysed at 800 °C for 2 hours with a heating and cooling ramp of 2 °C per second.

This procedure were repeated for three pore impregnations and three pyrolysis cycles since N_2 measurements showed that the pores still could be filled after the two first impregnations/pyrolysis steps.

3.2.2 Furfuryl amine

This materials will be referred to as C01:Px_2, C02:Px_2 and C03:Px_2, in which x_2 will be replaced with the number that corresponds to the level of how complete the material is. See table 3.2 for full material nomenclature.
In order to try to gain a C-N-Fe bond the FA is now changed to furfuryl amine (FAm) with the adding of $FeCl_3$ as iron source. There are three different samples in order to produce one iron free nitrogen containing reference and the two different ways of adding the iron, either dissolve it in the catalyst or in the FAm itself.

The C02 and C03 samples were produced exactly like the C00 with three major differences.

1. FAm (Fluka, $\geqslant$98.0% (GC)) were used as carbon source
2. In the C02 the FAm were as close to saturated with $FeCl_3$ as possible while the C03 were iron free

3. After the last carbon impregnation, the samples were divided into two parts where one part were treated normally and the other part were pyrolysed at 1100 °C instead of 800 °C

The C01 were treated a bit differently then the other two materials produced from FAm. Since the $FeCl_3$ were dissolved in the PTSA, the sample were not covered with catalyst but instead filled with an amount that matched the pore volume and then put to dry in a furnace at 80 °C for 2 hours. The dried sample were impregnated with FAm and pyrolysed the same way as C00 were when using FA.

3.2.3 Pyrrole

This material will be referred to as C04:Px_2, in which x_2 will be replaced with the number that corresponds to the level of how complete the material is. See table 3.2 for full material nomenclature.
One major difference with using pyrrole (Py) as carbon source is that there are no need for PTSA as catalyst since the $FeCl_3$ works as a catalyst on it's own. The $FeCl_3$ concentration should be as high as possible since [17] found a dependency between the amount of $FeCl_3$ in the pores and the the amount Py that were able to polymerize inside the pores. Though one should not exceed 2g $FeCl_3$ per 1g silica template since that will lead to deposition of Py on the outside surface instead of inside the pores (reference). To produce the C04 sample, 2g of OMS were impregnated with $FeCl_3$ in 1M HCl matching the pore volume. The $FeCl_3$ were dissolved in 1M HCl (type, 37% diluted in MilliQ) as 7.6M giving 1.36g per 1g OMS. The silica were dried in oven for 2 hours at 80 °C and then impregnated with Py with an amount that equalled the pore volume. The sample were then pyrolysed at 800 °C, as all previously samples. The sample were reimpregnated two more times and the last time, half of the sample were pyrolysed at 1100 °C instead of 800 °C.

3.2.4 Acrylonitrile

This materials will be referred to as C05:Px_2 and C06:Px_2, in which x_2 will be replaced with the number that corresponds to the level of how complete the material is. See table 3.2 for full material nomenclature.
The last carbon source chosen were acrylonitrile (AN) with AIBN as initiator and $FeCl_3$ dissolved in 1M HCl as iron source. Since the amount of OMS were beginning to run short, only 1.5 g silica were used for each of these batches. They were both prepared in the same way with the difference that the CS06 sample had a pretreatment step of 200 °C before pyrolysis.

1.5 grammes of OMS were impregnated with $FeCl_3$ dissolved in 1M HCl ($[FeCl_3]$ = 7.6M) and dried in an oven at 80 °C. When the silica were dry, the pores were filled with an amount of AN almost representing the pore volume of the silica. then some AIBN were dissolved in a small amount of AN and added to the silica. The impregnated silica were taken to the pyrolysis furnace where it were put to polymerise at 50 °C for 12 hours followed by a raise in temperature to 60 °C for 8 hours in an inter atmosphere. After the polymerisation step were carried out, the furnace were directly heated to pyrolysis temperature in the C05 case. In the C06 case the furnace were first heated to 200 °C for a pretreatment step before heating to pyrolysis temperature. As in previous synthesises, the pyrolysis temperature were either 800 °C for the "low" temperature pyrolysis or 1100 °C for the high temperature pyrolysis. Since the furnace couldn't be programmed to all of the steps required to have both the 50 °C, 60 °C and 200 °C step at the same time, the C06 polymerisation sequence were kept at 55 °C for 20 hours instead.

Another note is that since when the C05:P1 version of the material were done, the N_2 adsorption showed that the pores were more filled then after three impregnation-pyrolysis steps for the earlier materials. This made the C05 and C06 samples to be considered complete after only one impregnation-pyrolysis, and thus the silica were removed without any reimpregnations.

3.2.5 Pyrolysis temperature sequences

For the C00 to C04 materials, the pyrolysis procedure were the same. First the furnace were heated from room temperature up to 800 °C with 2 °C min^{-1}. Upon reaching the target temperature, this

temperature were held for 2 hours followed by controlled cooling down to room temperature with $-2\,^{\circ}\mathrm{C}$ min^{-1}. The same sequence were used for the CH1 to CH4 materials, with the difference that the target temperature were changed to $1100\,^{\circ}\mathrm{C}$. For the C05 and C06 material, a slight different sequence were used. For the C05 and CH05, the materials were first heated to $50\,^{\circ}\mathrm{C}$, $2\,^{\circ}\mathrm{C}$ min^{-1} and held there for 8 hours. Proceeding this, the temperature were then raised to $60\,^{\circ}\mathrm{C}$ by $2\,^{\circ}\mathrm{C}$ min^{-1} and upon reaching this temperature were held for 12 hours. After this low temperature pretreatment to let the material polymerize, the temperature were raised to the target pyrolysis temperature ($800\,^{\circ}\mathrm{C}$ for C05 and $1100\,^{\circ}\mathrm{C}$ for CH5) by $2\,^{\circ}\mathrm{C}$ min^{-1} and held there for 2 hours. When the pyrolysis were done, the furnace were cooled by $-2\,^{\circ}\mathrm{C}$ min^{-1} to room temperature. The C06 and CH6 materials were treated as the C05 and CH5 material but with the difference that there were an additional pre-treatment step between the polymerisation step and the pyrolysis step and. This additional step were reached by heating with $2\,^{\circ}\mathrm{C}$ min^{-1} to $200\,^{\circ}\mathrm{C}$.

4 Analytical Techniques

Different analytical techniques have been used in order to characterize the materials. The theory behind them are presented below.

4.1 N_2 physisorption

BET is a method for characterizing the specific pore volume, pore surface and pore size distribution of a sample using N_2 adsorption. The theory were developed by Brunauer, Emmett and Teller [3] which is an improvement of Irving Langmuirs theory of monolayer adsorption of gasses on surfaces making it a theory that accounts for multilayer adsorption.

$$\frac{1}{V(P_0/P-1)} = \frac{P}{P_0} \cdot \frac{C-1}{V_m C} + \frac{1}{V_m C} \tag{4.1}$$

C = BET constant calculated by the inclination and intersect in figure 4.1
P = equilibrium pressure
P_0 = saturation pressure
V = adsorbed gas quantity
V_m = mono layer adsorbed gas quantity

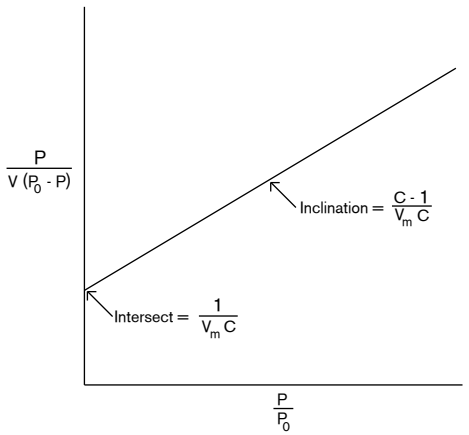

Figure 4.1: The BET curve used to calculate the BET constant C

The BET equation (eq 4.1) is based on the assumptions that:

1. A gas adsorbs physically to a surface forming infinite amounts of adsorption layers
2. There is no interaction between the adsorbed layers
3. Langmuirs theory is exertable on each layer formed

In order to calculate the specific surface, equation 4.3 is used.

$$S_{tot} = \frac{V_m N_A a_m}{V} \tag{4.2}$$

$$S = \frac{S_{tot}}{m} \tag{4.3}$$

a_m = the projected area of each molecule (16.2 Å^2 for N_2)
N_A = Avogardos number
V = molar volume of adsorbed gas
m = weight of the sample

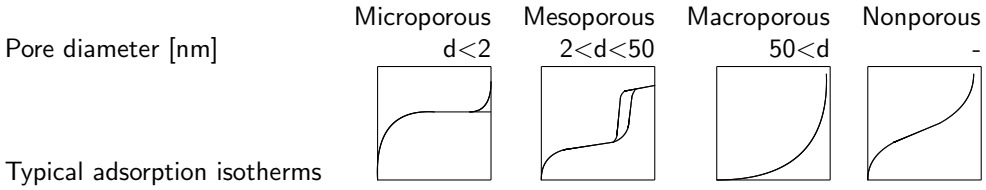

Figure 4.2: Classification of pores depending on their diameter. In the mesoporous area, the typical adsorption isotherm shows a hysteresis caused by irreversible capillary condensation. The appearance of the nonporous isotherm is caused by small primary particles (which adsorbs large quantities in low partial pressure). Images are reprinted from Brunauer et al. [3]

Pore size distribution of the sample is calculated using the BJH method. This method were developed by Barrett, Joyner and Halenda [1] by modifying Kelvin's equation to correct it for multilayer adsorption, yielding equation 4.4. This is one of the most used methods for determining the pore size distribution [9].

$$\ln \frac{p}{p_0} = \frac{-2\gamma V_L}{RT} \cdot \frac{1}{r_m} \tag{4.4}$$

4.2 Electron Microscopy

Electron Microscopy comes as two variants. Scanning- and Transmission Electron Microscopes (SEM and TEM). Electron microscopes are, basically, an optical microscope in which the beam for irradiation has been switched to electrons instead of photons and thus the lenses have been switched from optical lenses to magnetic lenses. This gives the TEM and SEM the advantage of much better resolution then an optical microscope (which is limited by the wavelength of the visible light) since the wavelength of electrons is much smaller. An optical microscope can see things that are as small as on the μm scale since the optical light used have a wavelength of 350 to 700 nm. The electron microscopes, on the other hand, can resolve objects that are in the nm-regime

4.2.1 SEM

In a SEM, the electron beam analyses the surface and the bulk down to a depth of approximately 1 μm of the sample. A SEM usually utilizes different side equipment, such as a detector for Energy-dispersive X-ray spectroscopy (EDX). EDX works in the same way as XPS but register the x-rays emitted from the sample instead of the Auger electrons forced away from the sample. A SEM combined with a EDX can give material composition information for the area scanned and can map the different materials on the image of the area and thus give a visual report of where the atoms are located.

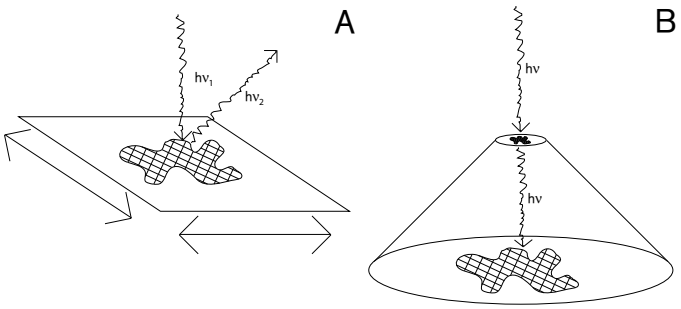

Figure 4.3: Schematic image of the difference between a SEM (A) and a TEM (B)

4.2.2 TEM

A TEM uses, as the name implies, transmission of the electron beam to analyse the specimen. This means that the sample needs to be thin enough to let the electrons transfer trough, which can be difficult to achieve in some cases. Figure 4.2 (B) shows a crude schematic of a typical TEM. The electron beam comes from an electron source and irradiates the specimen. Those electrons that are transmitted are magnified on a fluorescent screen or, in modern TEM, a computer screen.

4.3 Small and Wide Angle X-ray Scattering

Both SAXS, small angle x-ray scattering, and WAXS, wide angle x-ray scattering, utilize the same theory and only differs as the name applies that one of them uses small angles and the other wide angles. The theory behind scattering is that when the sample is hit by x-rays, the x-rays are divert a little bit from their path by the electrons in the material [14]

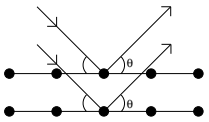

Figure 4.4: Typical schematic of interference. The dots represent some sort of order, e.g. pores in the sample, atoms in an crystalline structure of the sample, etc.

$$n\lambda = 2d \cdot \sin\theta \tag{4.5}$$

Usually SAXS operates at angles lower then 10 ° and WAXS at angles higher, but this is not a fixed value and differences may occur between different SAXS and WAXS machines. The distance of order in the material can be calculated from bragg's law (eq 4.5) and with an x-ray wavelength of 1.55 Å, materials with order or inhomogeneities in the nm size scale can be measured. This means that at lower angles (SAXS) the pore order of an ordered mesoporous material can be examined and at higher angles (WAXS) the order of the atoms in the material can be examined.

4.4 Raman

Raman is a spectroscopical method that utilize the fact that most compounds are able to get a shift in their polarization, i.e. the electron cloud of the molecule is able to be deformed [10]. Almost all

compounds are able to do this due to the fact that there are differences in the electron densities

The basics in the technique is that the sample is illuminated by a laser operating in the region between near IR to near UV. The photons are not absorbed but makes the electron oscillate and the photons either enter and leave the compound with the same energy as they were introduced with (yielding Rayleigh scattering) or some energy gets absorbed by either the photon or the molecule (yielding Stokes and anti-Stokes scattering), see figure 4.4.

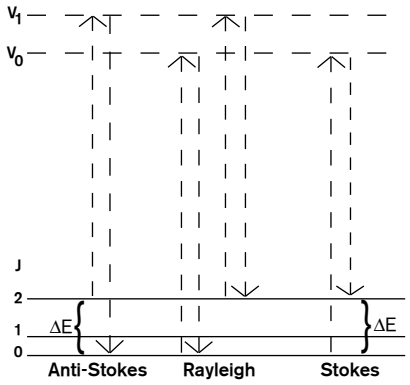

Figure 4.5: Image of the anti-Stokes, Rayleigh and Stokes scattering respectively. The V_0 and V_1 are virtual excitations states for the compound that are only used to explain the energy loss or gain during the Raman process. J levels are rotational states for the electrons. The selection rule for Raman is that $\Delta J = 0, \pm 2$

The benefit with Raman is that it is possible to make benefit of the internal vibrations and rotations of the molecules. Therefore it is usually easy to find unique peaks for different types of materials since most materials have "fingerprint patterns" which make them identifiable.

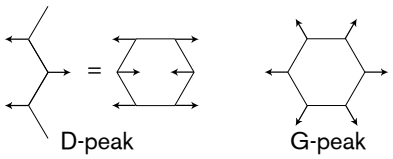

Figure 4.6: The cause of the Raman D-peak respectively the Raman G-peak in carbon materials. The "ring breathing" can only occur in graphite and other cyclic carbon materials while the ring stretching can be mistaken for chain stretching.

In the case of carbon materials, both amorphous and graphite content is identified in the Raman spectrum, as the D-peak (at 1310 cm^{-1}) and the G-peak (at 1580 cm^{-1}), respectively. The G-peak cannot occur in amorphous carbon due to that it is caused by "ring breathing" of the carbon rings, se figure 4.4. The D-band in figure 4.4 can be seen in chains as well and are thus present in amorphous carbon too [6].

4.5 X-ray Photoelectron Spectroscopy

X-ray Photoelectron Spectroscopy (XPS), also known as ESCA (Electron Spectroscopy for Chemical Analysis), is (mainly) a surface analysing method. It collects data of a depth of 1 to 10 nm on the

specimen surface and can in a sample analyse quantities of parts per thousands of almost all elements. The sample is attached to a small tape and put into a vacuum chamber. The sample is then irradiate with x-rays which knocks out electrons from one of the inner layers of electrons in the different atoms in the sample. To compensate for this, an electron in an outer orbital falls down to occupy the "hole". Usually this means that some excess energy can be transmitted, either as a new x-ray from the electron that falls down or to induce that a third electron moves. If the excess energy is transferred to one of the outer electrons, this electron may be forced away from the sample. An electron ejected in this way is referred to as an Auger electron. Each electron that reaches the detector is sorted by the kinetic energy it has when reaching the detector and counted by it and the kinetic energy an electron receives is proportional of the bonding energy of the atom it comes from which means that it is possible to tell different atoms apart as well as which the neighbouring atoms are [10].

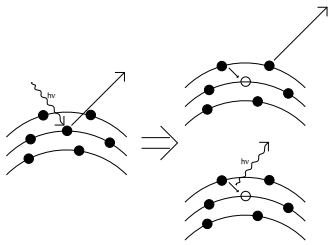

Figure 4.7: The incident x-ray beam knocks one electron away. To compensate for this loss, one outer electron takes the empty place by lowering its energy. The excess energy is either transmitted to a nearby electron, which forces it to leave or is disposed of as a new x-ray

5 Results

The results for the different materials are presented here. The mesoporous silica were all rather similar, with only smaller differences in the N_2 physisorption measurements. These differences are small enough to be random errors caused during the measurements and thus the silica batches can be considered similar.

5.1 OMS

	V_P [cm^3 g^{-1}]	S_{BET} [m^2 g^{-1}]	t-plot [m^2 g^{-1}]	t-$plot_{external}$ [m^2 g^{-1}]	Pore diameter (ads) [nm]
OMS01	1.07	763	252	511	7.31
OMS02	1.12	792	287	505	7.35

Table 5.1: N_2 physisorption data of the different OMS batches used

In figure 5.1, the SAXS data of the ordered mesoporous silica that were used as template are compared, showing that they both have long range ordered pores.

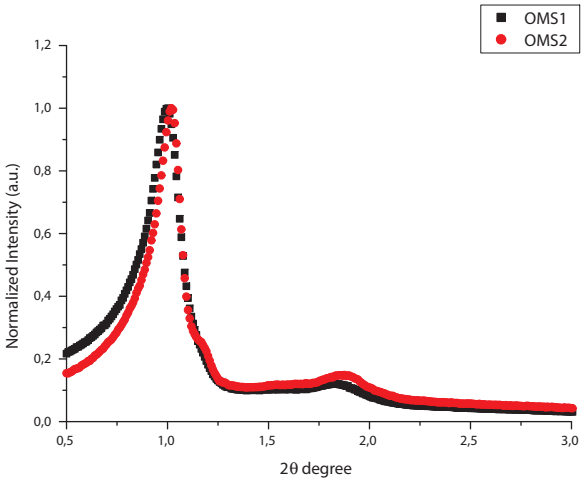

Figure 5.1: SAXS Analysis of the ordered mesoporous silica showing cubic ordered pores

Figure 5.2 displays the comparisons of one of the silica templates as well as the FA and Py material. The C01 and OMS that are compared in figure 5.2 resembles each other well. The reason for the shift between the silica and carbon curves is because the carbon is the inverted structure of the silica and have a smaller pore distance which means that it needs a little larger angles to be analysed (compare with equation **??**).

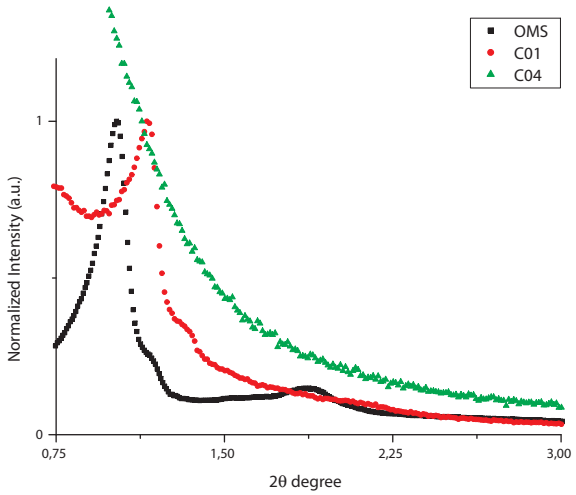

Figure 5.2: Comparing the OMS with C01 and C04, showing that the pore order of the carbon differs between the different carbon precursors

5.2 Furfuryl alcohol

The reference sample with pure carbon shows fairly good results. The N_2 physisorption measurement shows that the carbon produced have a similar characteristics as the silica template used. It differs some in the pore volume, pore diameter and the micropore area but are otherwise just as the template. The difference is not that extreme considering that the carbon material is an inverted replica of the OMS and thus should have the OMS wall thickness as pore volume.

	V_P [$cm^3\ g^{-1}$]	S_{BET} [$m^2\ g^{-1}$]	t-plot [$m^2\ g^{-1}$]	t-$plot_{external}$ [$m^2\ g^{-1}$]	Pore diameter (ads) [nm]
OMS	1.07	763	252	511	7.31
C00:P6	0.73	797	112	685	3.66

Table 5.2: N_2 physisorption data of the samples produced with FA as carbon source

Since there are neither iron nor nitrogen present in the synthesis, the EDX data shows none and besides from showing that not all of the silica were dissolved and not all PTSA were washed out of the pores, the material produced is more or less pure carbon.

	Carbon [A%]	Oxygen [A%]	Silica [A%]	Nitrogen [A%]	Iron [A%]	Sulphur [A%]	Fe/N
SEM-EDX							
C00:P6	93.43	6.30	0.16	-	-	0.12	-
XPS							
C00:P6	96.72	3.09	-	-	0.19	0	-

Table 5.3: SEM-EDX data of the samples produced with FA as carbon source

Figure 5.3: TEM image of C00. There are order in the material (as seen in figure 5.4) but unfortunately this order did not transfer well when taking the TEM image

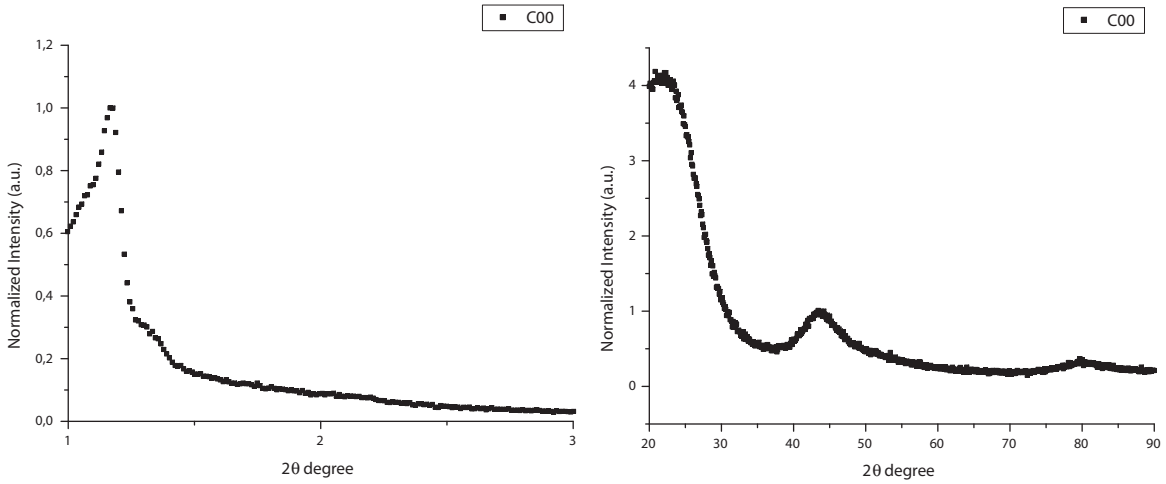

Figure 5.4: SAXS analysis of C00 to the left and WAXS analysis to the right. The SAXS analysis shows an well ordered pore structure when FA is used as precursor, while the WAXS analysis shows that there are graphite boundaries in the material

WAXS of the FA based material suggests that there are graphite in the material, but not whether it's thoroughly graphite or if it's just graphitic areas that the WAXS sees, se figure 5.4. Raman suggests also that there are graphite in the material (se figure 5.5), but since the analysis is too dependant on where in the material it is performed, it is impossible to say how much of the material that is graphitic.

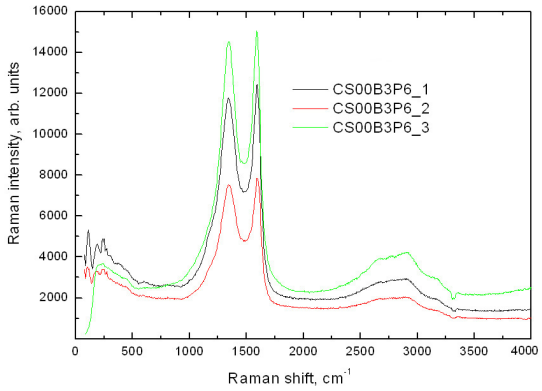

Figure 5.5: Raman spectra of C00:P6

The XPS images does not show anything unexpected, the overview spectra shows some carbon, oxygen and sulphur while the close-up of the carbon peak reveals that there are both C-C (the big peak to the right) and C-O (the smaller peak second to the right) bonds. What the other peaks shows are different kind of carbon bonds to oxygen as well as C-S.

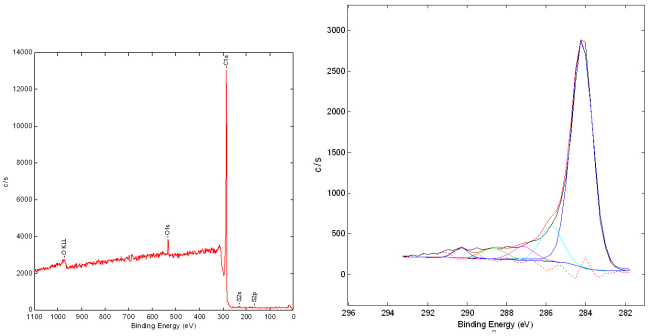

Figure 5.6: XPS overview spectra of C00:P6 to the left and close-up spectra of the carbon peak to the right

5.3 Furfuryl amine

	V_P [cm^3 g^{-1}]	S_{BET} [m^2 g^{-1}]	t-plot [m^2 g^{-1}]	t-$plot_{external}$ [m^2 g^{-1}]	Pore diameter (ads) [nm]
OMS	1.07	763	252	511	7.31
C01:P6	1.26	1014	153	860	3.86
CH1:P6	1.35	1101	93	1008	3.75
C02:P6	1.07	1187	-	1187	3.16
CH2:P6	1.05	1211	-	1211	2.98
C03:P6	1.18	1108	27	1080	3.4
CH3:P6	0.97	1098	24	1074	3.00

Table 5.4: N_2 physisorption data of the samples produced with FAm as carbon source

	Carbon [A%]	Oxygen [A%]	Silica [A%]	Nitrogen [A%]	Iron [A%]	Sulphur [A%]	Fe/N
EDX Data							
C01:P6	81.25	44.74	0.09	7.34	1.65	0.38	0.225
CH1:P6	88.09	49.45	0.49	4.75	0.03	0.45	0.007
C02:P6	84.32	40.08	0.33	7.76	0.08	0.48	0.011
CH2:P6	88.02	54.42	0.67	4.04	0.00	0.51	-
C03:P6	84.38	42.38	0.30	7.70	-	0.31	-
CH3:P6	86.75	57.47	0.72	4.37	-	0.28	-
XPS Data							
C01:P6	82.47	10.76	0	3.03	3.43	0.31	1.133
CH1:P6	96.39	2.46	0	0.95	0.01	0.19	0.011
C02:P6	92.88	3.55	0	3.29	0	0.28	-
CH2:P6	94.97	3.98	0	1.05	0	0	-
C03:P6	93.95	3.37	0	2.69	-	0	-
CH3:P6	94.09	5.26	0.49	0	-	0.16	-

Table 5.5: SEM-EDX and XPS data of the samples produced with FAm as carbon source

The FAm samples show some N and Fe content in the C01 and C02 materials, unfortunately there have been no verification of whether there are C-N-Fe bonds since the XPS overview spectra are not resolved enough (see figure 5.10). The XPS result confirms that there are either C-O or C-N bonds (it is most likely that both bonds exist) since they both have shift near 1 to 1.5 from the C-C bonds, se figure 5.10. It is, however, not possible to see the difference between the C-O and C-N peaks since they are too close together and since all of the close-up spectrum of all materials look the same, it's not possible to make any conclusions of what the peaks consists of even if one have knowledge of what kind of atoms the material contains.

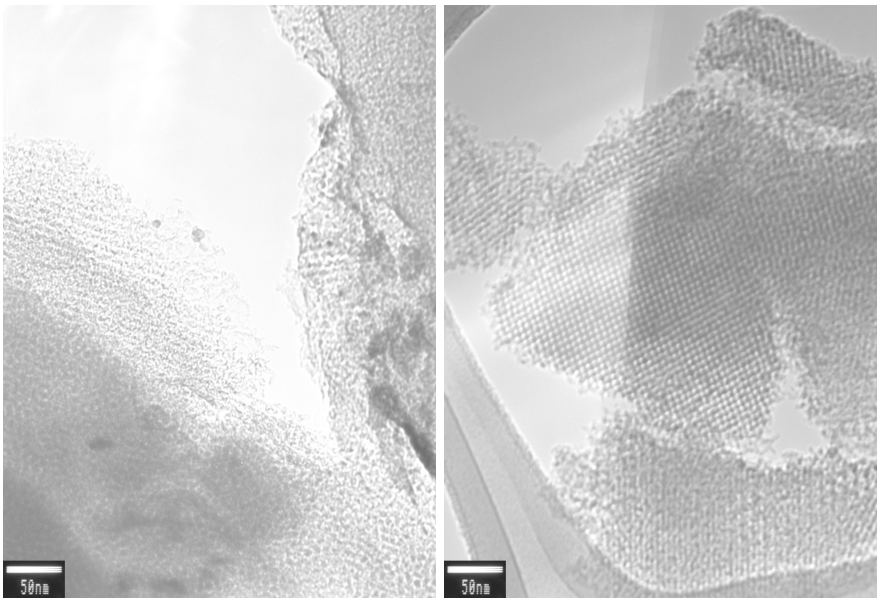

Figure 5.7: TEM image of C01 and CH1. The order of the pores are not easily seen, though SAXS suggests that there are order (se figure 5.11). The dark dots in the left image might be the cohenite discussed in section 5.7 or might just be areas where there are a slightly thicker layer of carbon then the rest of the sample

The TEM images of the materials shows somewhat the same thing as the SAXS confirms, that there are order in the FAm materials with Fe (with somewhat reduced order when the Fe were presented into the pores at the same time as the FAm) and that there are no order in the FAm sample without iron precursor. The pore order in the images are not easily seen since the photographing of the samples seem

to have disrupted the sample and the clear view of the order lost, which means that to confirm the order, the SAXS data should be the one to be trusted.

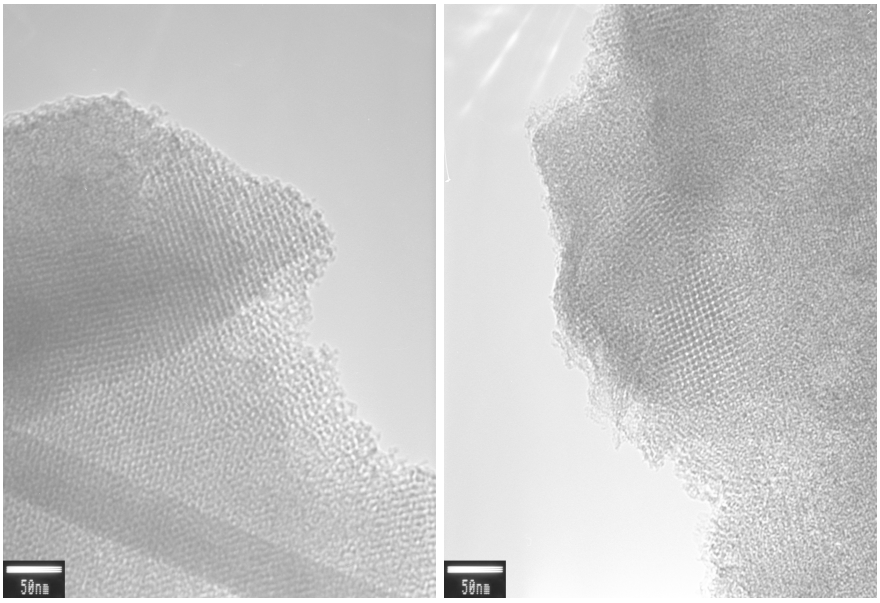

Figure 5.8: TEM image of C02 and CH2. The pores in the C02 sample may seem more ordered the the pores in the C01 sample, but are in fact not according to SAXS analysis

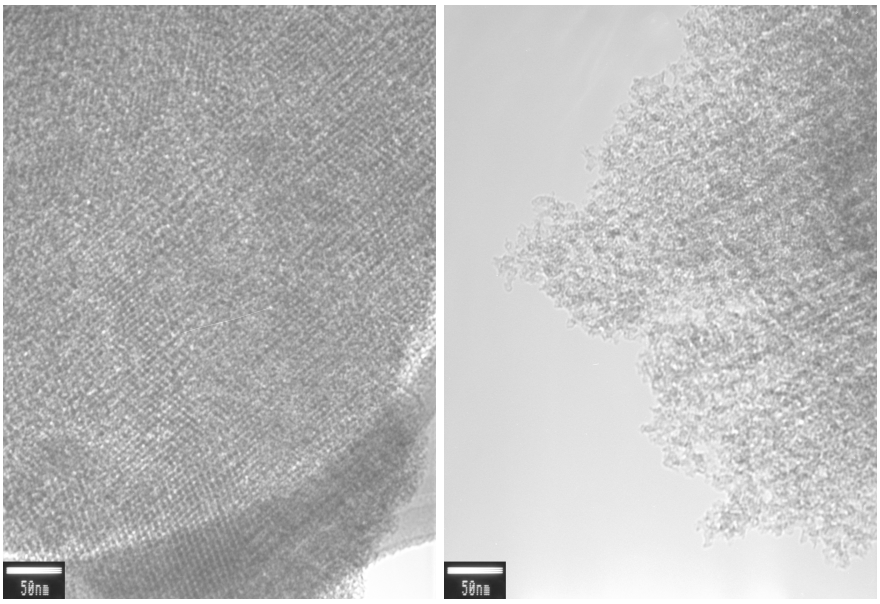

Figure 5.9: TEM image of C03 and CH3. There are some areas that seem to be a bit ordered, but most of the pores are amorphous

In figure 5.10 the left overview spectra is to "messy" to certainly know whether if there are any C-N-Fe bonds or not. In the right close-up spectra, the big peak is the C-C bonds while the small peak just to the left of the C-C peak is either C-O or C-N, which said above is not possible to tell apart.

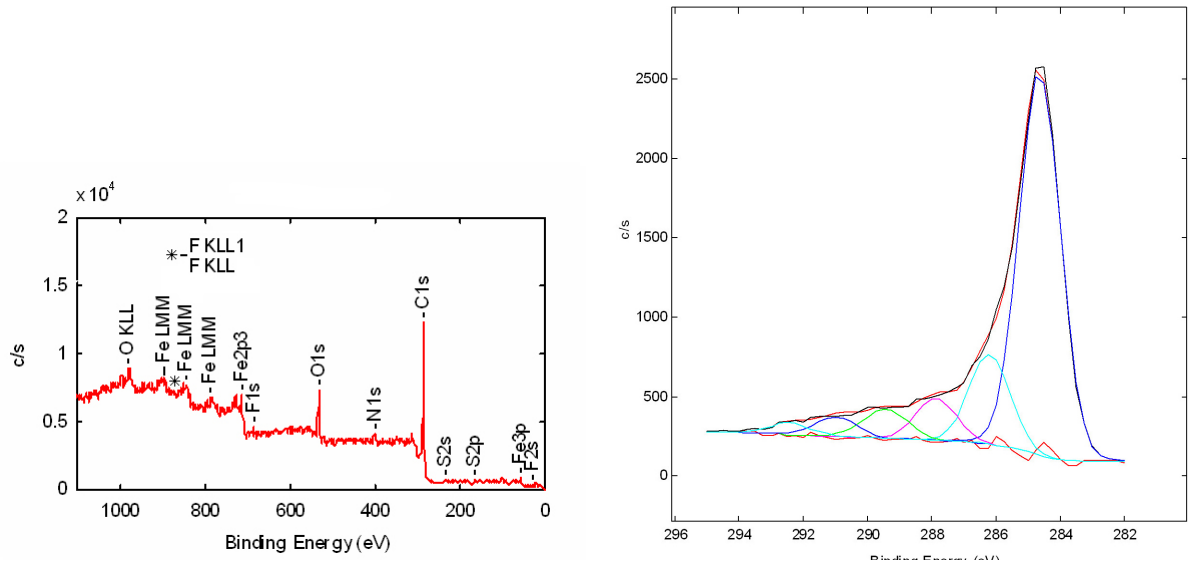

Figure 5.10: XPS overview spectra of C01:P6 to the left and an close-up spectra of the carbon peak to the right

The SAXS analysis in figure 5.11 reveals different ordered pores depending how the iron were presented into the silica template pores. The C01 and CH1 have a clearly ordered pore structure while C02 and CH2 have order together with amorphous areas. There are indices that some of the pores in the C03 and CH3 material is ordered, but most of the pores are amorphous. The WAXS analysis of C01:P6 to CH3:P6 shows that there are graphite boundaries from both 800 °C and 1100 °C temperature treatment. The C01 also show some unexpected peaks that are discussed in section 5.7

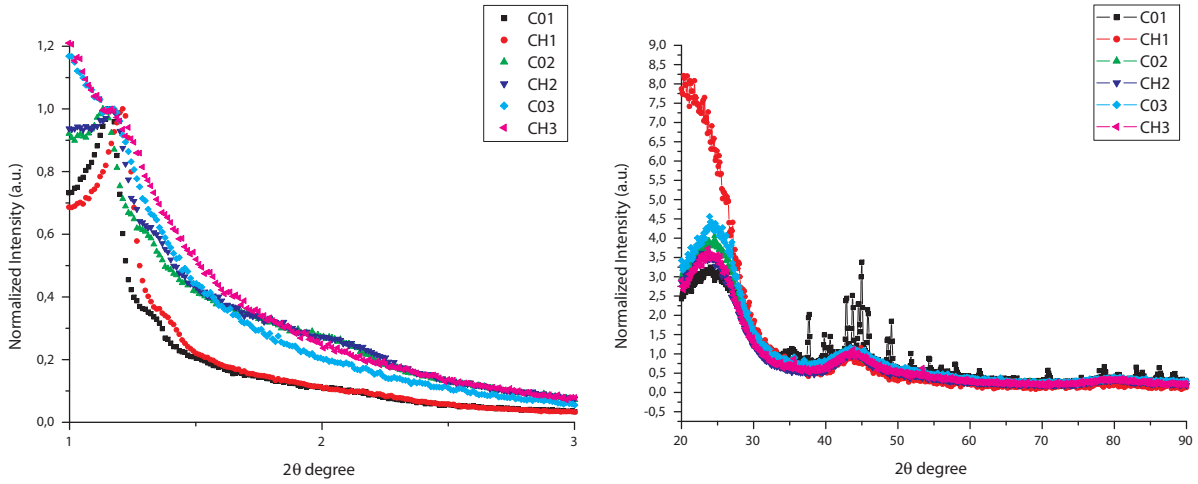

Figure 5.11: SAXS and WAXS analysis of C01:P6 to CH3:P6.

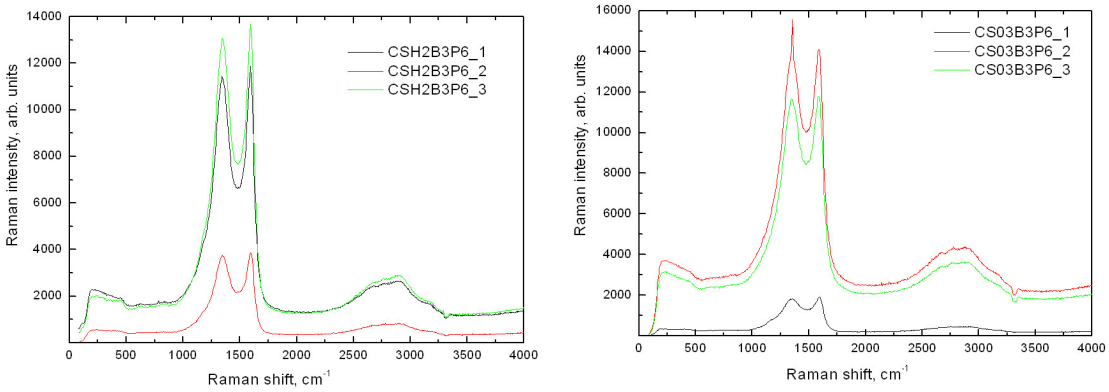

Figure 5.12: Raman spectra of CH2:P6 and C03:P6 showing that the measurement depends on where in the material the analysis were performed

5.4 Pyrrole

The analysis of C04 and CH4 gives a little bit different results depending on whether which method used. The SEM-EDX gives an Fe to N ratio of 0.67 while the XPS analysis set the ratio to be 2.58. This differs quite a lot as values, but both are probably correct. The XPS covers an area of 500×500 μm and penetrates the sample at a depth of 4 to 9 nm. The EDX covers approximately the same area but penetrates the samples deeper, about 1 μm. This makes the XPS measure the average composition of the surface and the EDX the average of the, more or less, entire sample and since iron were presented into the OMS pores before the pyrrole, it likely to believe that the iron are at a larger concentration in the sample surface. Since the nitrogen is presented into the OMS pores at the same time as the carbon (since it's chemically bound to the carbon) it is likely to show a higher concentration if a deeper analysis penetration is done. Thus the ratio of Fe to N will be severely different even though both analysis methods probably are correct. This would also explain why the XPS results show no silica, since the only undissolved silica in the sample are located deep within the pores of the carbon.

	V_P [cm^3 g^{-1}]	S_{BET} [m^2 g^{-1}]	t-plot [m^2 g^{-1}]	t-$plot_{external}$ [m^2 g^{-1}]	Pore diameter (ads) [nm]
OMS	1.12	792	287	505	7.35
C04:P6	0.66	605	385	220	2.09
CH4:P6	0.91	861	468	393	2.09

Table 5.6: N_2 physisorption data of the samples produced with FA as carbon source

	Carbon [A%]	Oxygen [A%]	Silica [A%]	Nitrogen [A%]	Iron [A%]	Sulphur [A%]	Fe/N
EDX Data							
C04:P6	75.20	61.46	0.10	4.87	3.27	0.29	0.671
CH4:P6	92.97	91.17	0.13	0.00	0.08	0.40	-
XPS Data							
C04:P6	69.32	19.29	0	3.18	8.21	0	2.580
CH4:P6	96.43	2.17	0	0.98	0.23	0.19	0.235

Table 5.7: SEM-EDX and XPS data of the samples produced with Py as carbon source

The C04 material shows, by far, the highest Fe to N ratio of all samples. Unfortunately, it is the same as for the FAm material, there have been no verification of whether there are any C-N-Fe bonds in the material. The XPS result still confirms that there are either C-O or C-N bonds and it is in this case still likely that both bonds exist at the same time since both O and N are present in the sample.

The EDX and XPS data in table 5.4 reveals that this method is good for inducing both N and Fe in the material. There are however two conclusions one can make from the results of pyrrole and furfuryl amine. One is that a high temperature treatment severely reduces both the N and Fe content (both table 5.4 and table 5.5 from the FAm materials show this). The second conclusion is that pyrrole does not produce ordered pores, see SAXS data in figure 5.15. Even the TEM images of the Py based materials show that they are totally amorphous since the materials mostly look "fuzzy". There are darker areas in the C04 material in figure 5.13 can be cohenite, which was an unexpected result in the C01 and C04 materials. This is discussed more in section 5.7.

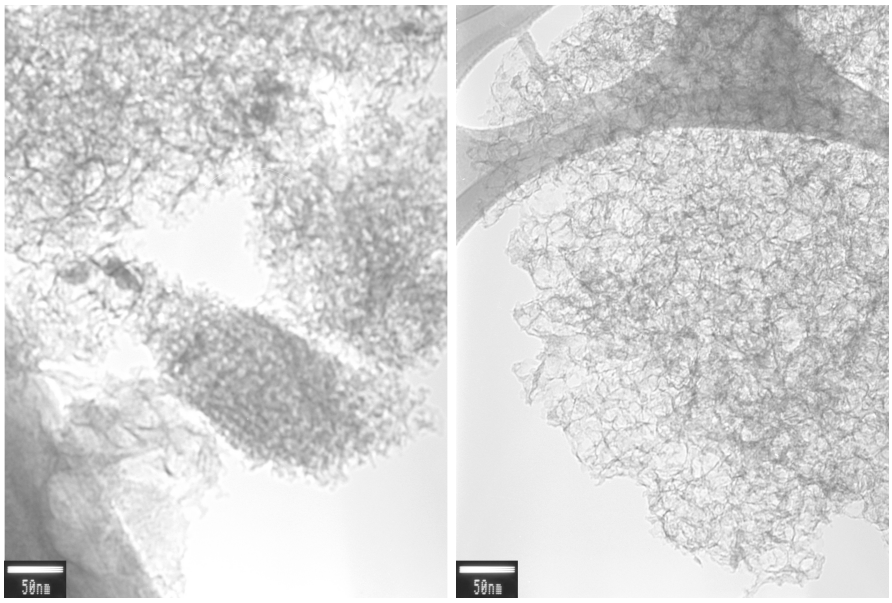

Figure 5.13: TEM image of C04 and CH4. There are darker areas in the C04 sample that might be cohenite (se section 5.7)

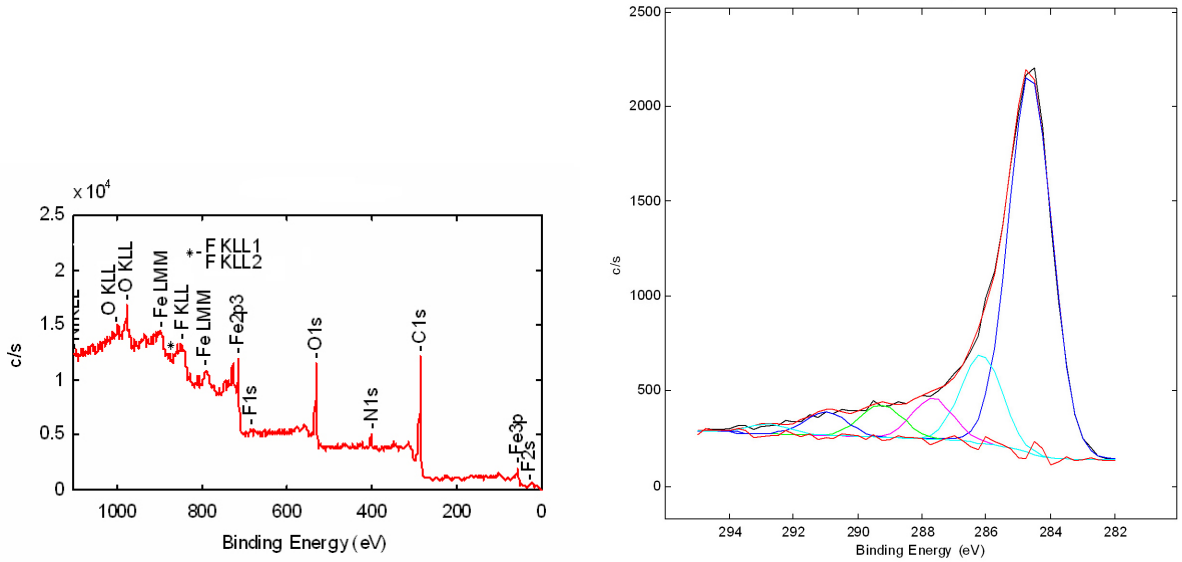

Figure 5.14: XPS overview spectra of C04:P6 to the left and the and close-up of the carbon peak to the right

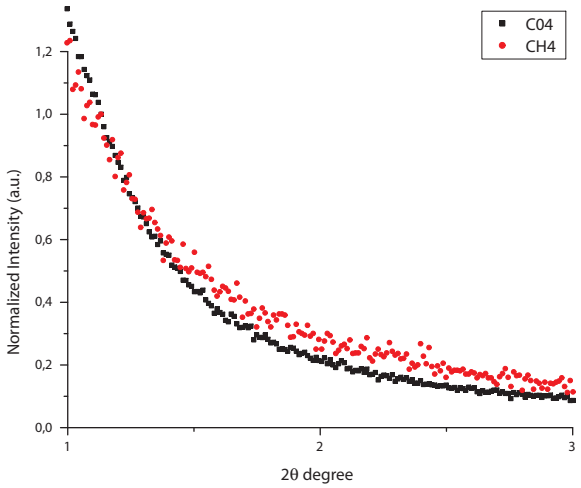

Figure 5.15: SAXS analysis of C04:P6 and CH4:P6 reveals totally amorphous pore order

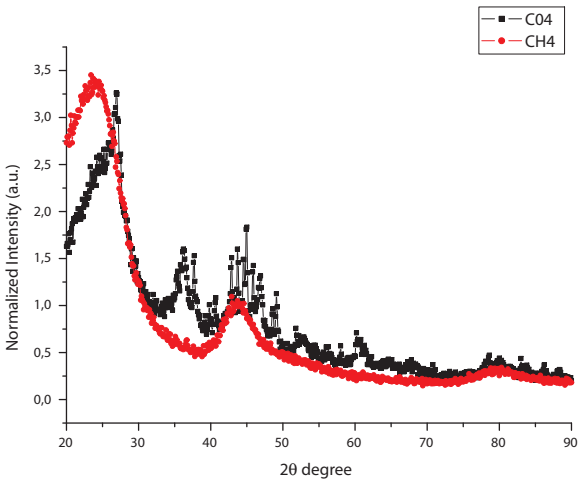

Figure 5.16: WAXS analysis of C04:P6 and CH4:P6 shows that there are graphite boundaries from both 800 °C and 1100 °C temperature treatment. The C04 also show some unexpected peaks that are discussed in section 5.7

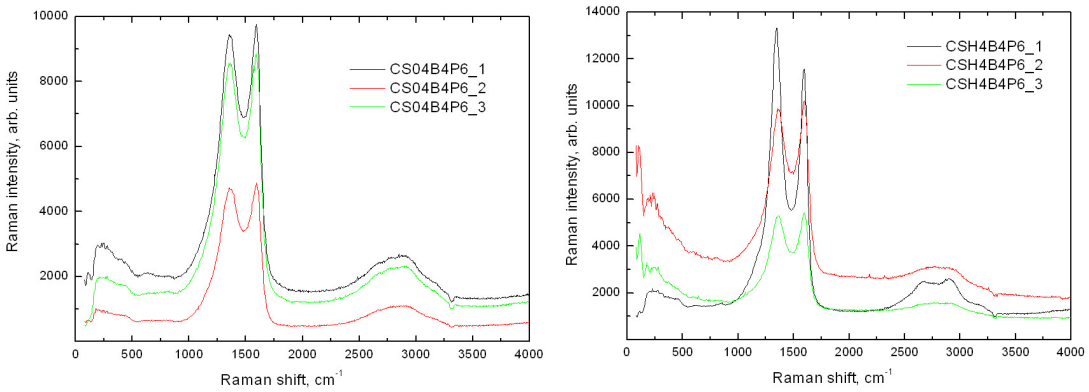

Figure 5.17: Raman spectra of C04:P6 and CH4:P6

5.5 Acrylonitrile

The acrylonitrile based materials were a bit difficult to analyse since there were not much material left after the silica removal. None of the materials were so abundant that is was possible to perform an N_2 physisorption of them. It was possible to perform most of the other analysis and the result are presented below.

	Carbon [A%]	Oxygen [A%]	Silica [A%]	Nitrogen [A%]	Iron [A%]	Sulphur [A%]	Fe/N
EDX Data							
C05:P6	Insufficient material						
CH5:P6	89.45	89.39	0.66	0	0.07	0.38	-
C06:P6	87.49	92.09	0.66	0	0.14	0.18	-
CH6:P6	Insufficient material						
XPS Data							
C05:P6	Insufficient material						
CH5:P6	92.86	5.29	0	1.85	0	0	-
C06:P6	84.52	12.66	0	2.82	0	0	-
CH6:P6	Insufficient material						

Table 5.8: SEM-EDX and XPS data of the samples produced with AcN as carbon source

The result from the EDX and XPS are a bit odd. As concluded in the result of the Py based materials (section 5.4) the EDX should show a higher amount of nitrogen then the XPS and vice versa, the XPS should show a higher amount of iron present. In this case it is the total opposite even though the iron were presented into the pores before the acrylonitrile. Why this result shows what it does, I cannot explain since it should be the opposite. It can be because the material synthesized were so scarce that the analysis is not reliable. If the result are reliable, then the conclusion drawn must be that acrylonitrile is a difficult media to induce C-N-Fe bonds in since the amounts of both N and Fe are low.

The TEM images of the materials were quite interesting. There were several darker areas that blinked when exposed to the electron beam. They resembles the darker areas in the C01 and C04 materials, but since the SAXS analysis of the AcN based materials (figure 5.19) does not show the same “spikes” peaks as in neither the FAm (figure 5.11) nor Py (figure 5.15) based materials, these“dots” are most likely not caused by the same reason. Since these areas not can be considered caused by cohenite, they are probably either unreacted acrylonitrile that are present in the pores or iron that have agglomerated.

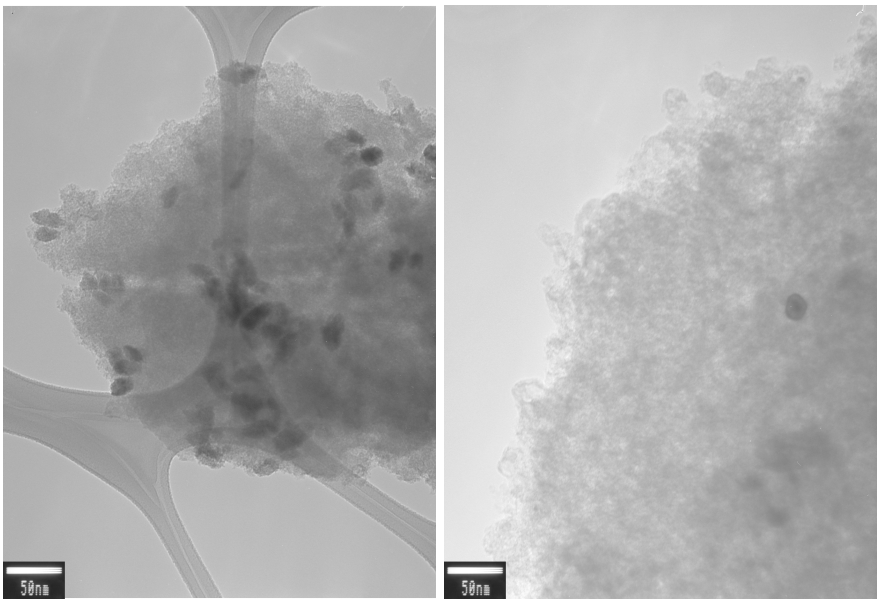

Figure 5.18: TEM image of CH5 and C06. There are darker areas in both samples are most likely not cohenite but either carbon precursor that have not reacted or iron agglomerates

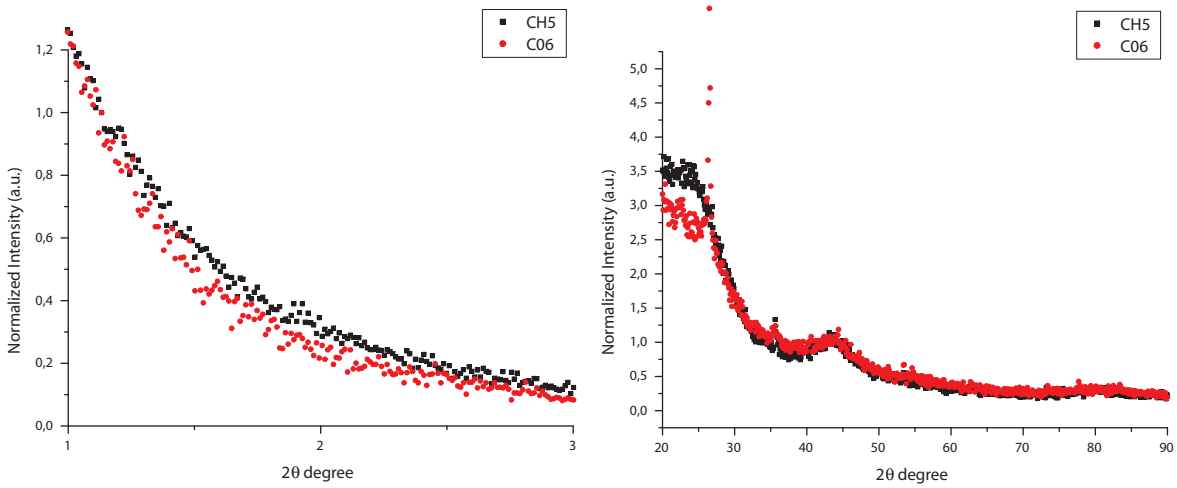

Figure 5.19: SAXS and WAXS analysis of CH5:P6 and C06:P6 respectively. The SAXS reveals totally amorphous pore order while the WAXS reveals graphite boundaries in both temperature treatments

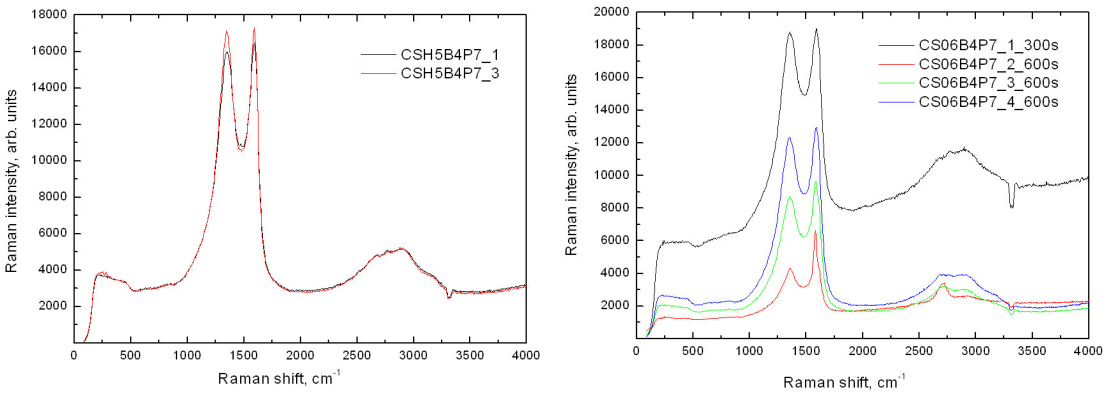

Figure 5.20: Raman spectra of CH5:P6 and C06:P6

5.6 Temperature treatment

The temperature treatments of the materials were performed by pyrolysing at either 800 °C or 1100 °C. The idea was that a higher temperature would produce graphite materials or at least a material that are more graphitizisesed then the lower temperature would. As seen in the WAXS data of the different materials is that both temperatures give rise to graphite areas in the materials. I could have been possible to tell the sizes of the graphite boundaries in Raman if it wasn't for that the Raman analysis depended too much of where in the material the analysis were performed. Thus, both temperatures produce materials with graphite content but it is impossible to say if there are more or less graphite areas in a particular material. The XPS and EDX analysis of the materials however reveal that a higher temperature seem to reduce the amount of both nitrogen as well as iron present in the materials. Greene et al. [8] show that a higher temperature should produce a material that are more graphitizised then a lower temperature, but until it is proven that it applies to these samples, the best conclusion must be to use a pyrolysis temperature of 800 °C. This conclusion is drawn since the higher temperature reduces the chances of getting enough C-N-Fe bonds for the material to be effective enough to be a real option as replacement for platinum in PEMFC.

5.7 Deviations

There were some odd results that appeared after pyrolysis in some materials. In the WAXS analysis of both C01 and C04 there are "spiked" peaks that does not appear in any other material. These are also the materials with the highest N and Fe content, which might be the reason for the result. The reference library for the XRD machine that performed the WAXS analysis suggested that these peaks could be cohenite (Fe_3C) that were synthesised in the pores. Cohenite appear naturally in iron rich meteorites and in volcanic stones in which the iron is chemically reduced from assimilation of graphite according to the Rruff project in the university of Arizona [5]. The scanned images of the WAXS analysis showing the expected bars from cohenite are shown in figure 5.21 and figure 5.22 which reveals an almost exact match from the peaks. Exactly how the presence of cohenite will affect the result and effectiveness of the material if it is used as catalyst in a PEMFC is right now unknown. It will either not affect at all or might either increase or decrease the effect. Since the results so far shows that it is the C-N-Fe bonds that have effect, the presence of cohenite might reduce the effectivity since it lowers the amount of C-N-Fe bonds, but it is not impossible that it actually helps the reaction. Without further testing, it is impossible to say for certain what the result will be.

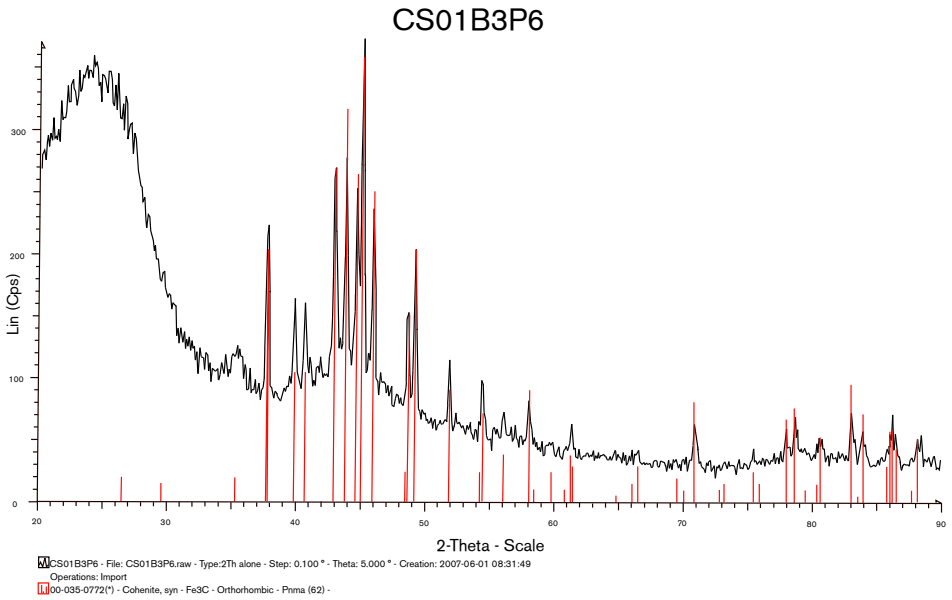

Figure 5.21: WAXS analysis showing cohenite in C01:P6

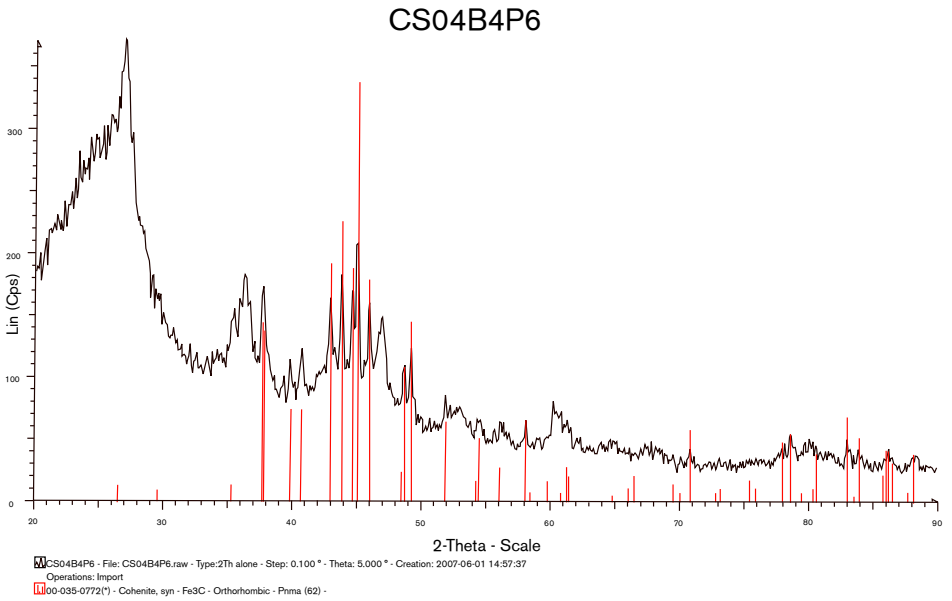

Figure 5.22: WAXS analysis showing cohenite in C04:P6

An other odd result in the materials were that in some of the high temperature pyrolysis the silica template seemed to migrate away from the designated sample holder. In figure 5.23 one of the ways the silica were migrating are shown. This did not occur in any of the 800 °C pyrolysis runs and thus must be a result of the high temperature. In one of the more severe cases the silica positioned itself right in front of the sample holders as a small half-sphere almost blocking the inert atmosphere flow. It is unlikely that it could black the flow completely since the flowrate would be to high and the pressure buildup would crack the silica wall, but it might affect the pyrolysis result. In the FAm and Py cases, it

does not appear as if these migrations made any differences in the materials produced, but might have been the reason for the low yield of the AcN based materials since the silica pores were filled a lot faster in these materials then in the other. In other words, the silica might have migrated and covered the pore entrances. This does, however, contradicts with the fact that this migration was only observed in the high temperature pyrolysis but it might be explained with that the AcN materials were in the same furnace for polymerisation before increasing the temperature for pyrolysis.

Figure 5.23: Silica template migrating away from the sample. Normally the carbon material in the sample holder should be entirely black and the walls of the sample holder should not be covered in white fuzzy silica

6 Conclusions

It should be noted that since none of the materials have been synthesized more then once, the conclusions drawn are based upon the assumption that the result is correct and will be reproducible. To completely verify the result, all materials need to be resynthesized.

From the results, one conclusion that can be seen is that the structural order depends on both the carbon precursor as well as the way the iron source were presented into the pores. When using FAm (material C01, C02 and C03) the SAXS data reveal a change in how well the pores are ordered. Since the only difference between the materials is how the iron source were presented to the silica template, i.e. dissolved in the PTSA (material C01), in the FAm (material C02) or not used at all (material C03), this result shows that the presence of iron affects the pore order. Comparing the FAm based material with the Py based material (comparing C01 to C04), the only difference is the carbon precursor (both materials have had the iron introduced into the pores before the carbon precursor) but still the C01 material have a well ordered pore structure while the C04 material is totally amorphous.

The second conclusion is that graphitization of the materials *may* be temperature dependant. Both Raman and WAXS data shows graphite boundaries in all of the materials independent of temperature treatment, but since the amount of graphite and amorphous carbon cannot be calculated (due to Raman being to sensitive to the analysis position in the sample), there might be more graphite content in the higher temperature treatment. The reason for this conclusion, without visible support from the Raman data, is that other work with graphitization reveals a temperature dependency and that materials usually gain more graphite content at higher temperatures [8]. So, in other words, 800 °C is enough to induce graphitization but a higher temperature *might* increase the amount of graphite content.

The third conclusion is that the nitrogen and iron content is lowered at higher temperatures. In all of the materials, the N and Fe content is lower in the materials undergoing a pyrolysis at 1100 °C then those undergoing pyrolysis at 800 °C. The lowering of the Fe content is most likely caused by atom migration of the iron

Summary:

- Carbon precursor and the way iron is introduced into the template pores will affect the pore order
- Graphitization *may* be temperature dependant
- Nitrogen and iron content is inversely proportional to the temperature

7 Acknowledgements

My deepest gratitude goes to the following persons:
Lic.Eng. Kjell Wikander For supervising and guiding me through my thesis work.
Professor Krister Holmberg For supervising and examination.
Assistant Professor Anders Palmqvist For additional supervision.
Senior Lecturer Lars Löwendahl and researcher Sven-Ingvar Andersson For helping me when the TriStar N_2 physisorption machine gave me trouble.
Research student Istaq Ahmed For showing me how to operate the pyrolysis furnace and letting me use it so frequently.
Senior Research Engineer Anne Wendel For helping me with the XPS measurements of my samples.
Visiting researcher Roman Holomb For helping me with the RAMAN measurements of my samples.
All persons at the dept. of TYK and KCK For accepting me as "one of the crew" and being so nice to me.
All of my friends For believing in me.
My family For your endless support and love.
Marie, my girlfriend For being there, loving me and making my work easier. I love you.

8 Appendix 1

8.1 N_2 physisorption data

	V_P [$cm^3\ g^{-1}$]	S_{BET} [$m^2\ g^{-1}$]	t-plot [$m^2\ g^{-1}$]	t-plot$_{external}$ [$m^2\ g^{-1}$]	Pore diameter (ads) [nm]
OMS01	1.13	791	260	531	7.32
OMS02	1.06	744	234	510	6.99
OMS03	1.07	763	252	511	7.31
OMS04	1.12	792	287	505	7.35
C00:P1	0.10	349	348	1	3.76
C00:P3	0.01	377	-	412	2.38
C00:P5	0.02	217	217	-	-
C00:P6	0.73	797	112	685	3.66
C01:P1	0.51	438	24	414	6.01
C01:P3	0.24	316	105	211	3.76
C01:P5	0.12	236	98	138	3.78
C01:P6	1.26	1014	153	860	3.86
CH1:P5	0.03	21	5	16	3.87
CH1:P6	1.35	1101	93	1008	3.75
C02:P1	0.61	486	110	376	5.81
C02:P3	0.39	320	68	252	5.82
C02:P5	0.24	238	64	174	5.30
C02:P6	1.07	1187	-	1187	3.16
CH2:P5	0.16	150	0.3	149.7	3.93
CH2:P6	1.05	1211	-	1211	2.98
C03:P1	0.59	418	28	390	6.10
C03:P3	0.45	369	62	307	5.62
C03:P5	0.33	299	74	225	5.27
C03:P6	1.18	1108	27	1080	3.4
CH3:P5	0.25	197	0.2	196.8	4.32
CH3:P6	0.97	1098	24	1074	3.00
C04:P1	0.18	233	150	83	2.11
C04:P3	0.17	226	154	72	2.08
C04:P5	0.14	193	135	58	2.14
C04:P6	0.66	605	385	220	2.09
CH4:P5	0.16	183	97	86	2.18
CH4:P6	0.91	861	468	393	2.09
C05:P1	0.01	2.8	-	2.8	2.11
C05:P7	Insufficient material	-	-	-	-
CH5:P1	0.21	56	5	51	2.16
CH5:P7	Insufficient material	-	-	-	-
C06:P1	0.16	54	6	48	2.24
C06:P7	Insufficient material	-	-	-	-
CH6:P1	0.01	4.7	0.3 4.4	2.14	
CH6:P7	Insufficient material	-	-	-	-

Table 8.1: Complete list of N_2 adsorption data. Due to difficulties in finding an accurate inflexion point in the P1 to P5 materials, these t-plots may be inaccurate

8.2 SEM-EDX data

	Carbon [A%]	Oxygen [A%]	Silica [A%]	Nitrogen [A%]	Iron [A%]	Sulphur [A%]	Fe/N
C00:P6	93.43	6.30	0.16	-	-	0.12 -	
C01:P6	81.25	44.74	0.09	7.34	1.65	0.38	0.225
CH1:P6	88.09	49.45	0.49	4.75	0.03	0.45	0.007
C02:P6	84.32	40.08	0.33	7.76	0.08	0.48	0.011
CH2:P6	88.02	54.42	0.67	4.04	0.00	0.51	-
C03:P6	84.38	42.38	0.30	7.70	-	0.31	-
CH3:P6	86.75	57.47	0.72	4.37	-	0.28	-
C04:P6	75.20	61.46	0.10	4.87	3.27	0.29	0.671
CH4:P6	92.97	91.17	0.13	0.00	0.08	0.40	-
C05:P7	Insufficient material						
CH5:P7	89.45	89.39	0.66	0.00	0.07	0.38	-
C06:P7	87.49	92.09	0.66	0.00	0.14	0.18	-
CH6:P7	Insufficient material						

Table 8.2: Complete list of SEM-EDX data, all values are atom-%. Values marked with a dash are defined as zero while a zero means that the detector didn't register any of this atoms

8.3 XPS data

	C1s [0.314]	O1s [0.733]	Si2p [0.368]	N1s [0.499]	Fe2p [2.946]	S2p [0.717]	Fe/N
C00:P6	96.72	3.09	-	-	0.19	0	-
C01:P6	82.47	10.76	0	3.03	3.43	0.31	1.133
CH1:P6	96.39	2.46	0	0.95	0.01	0.19	0.011
C02:P6	92.88	3.55	0	3.29	0	0.28	-
CH2:P6	94.97	3.98	0	1.05	0	0	-
C03:P6	93.95	3.37	0	2.69	-	0	-
CH3:P6	94.09	5.26	0.49	0	-	0.16	-
C04:P6	69.32	19.29	0	3.18	8.21	0	2.580
CH4:P6	96.43	2.17	0	0.98	0.23	0.19	0.235
C05:P7	Insufficient material						
CH5:P7	92.86	5.29	0	1.85	0	0	-
C06:P7	84.52	12.66	0	2.82	0	0	-
CH6:P7	Insufficient material						

Table 8.3: Complete list of XPS data, all values are atom-%. Values marked with a dash are defined as zero while a zero means that the detector didn't register any of this atoms

Bibliography

[1] Elliott P. Barrett, Leslie G. Joyner, and Paul P. Halenda. The determination of pore volume and area distributions in porous substances. I. computations from nitrogen isotherms. *Journal of the American Chemical Society*, 73(1):373–380, 1951.

[2] Rajesh Bashyam and Piotr Zelenay. A class of non-precious metal composite catalysts for fuel cells. *Nature*, 443(7107):63–66, 2006.

[3] Stephen Brunauer, P. H. Emmett, and Edward Teller. Adsorption of gases in multimolecular layers. *Journal of the American Chemical Society*, 60(2):309–319, 1938.

[4] Guido Busca, Luca Lietti, Gianguido Ramis, and Francesco Berti. Chemical and mechanistic aspects of the selective catalytic reduction of NO_x by ammonia over oxide catalysts: A review. *Applied Catalysis B: Environmental*, 18 (1-2):1–36, 1998.

[5] Rruff Project conducted at the Dept of Geosciences University of Arizona. Online database of raman spectra, x-ray diffraction and chemistry data for minerals, collected june 2007. URL `http://rruff.geo.arizona.edu/doclib/hom/cohenite.pdf`.

[6] A.C. Ferrari and J. Robertson. Interpretation of raman spectra of disordered and amorphous carbon. *Physical Review B*, 61(20):14095–14107, 2000.

[7] Antonio B. Fuertes and Dasha M. Nevskaia. Control of mesoporous structure of carbons synthesised using mesostructured silica as template. *Microporous and mesoporous materials*, 62:177–190, 2003.

[8] M.L. Greene, R.W. Schwartz, and J.W. Treleaven. Short residence time graphitization of mesophase pitch-based carbon fibers. *Carbon*, 40:1217–1226, 2002.

[9] J.C. Groen, L.A.A. Peffer, and Javier Pérez-Ramírez. Pore size determination in modified micro- and mesoporous materials. pitfalls and limitations in gas adsorption data analysis. *Microporous and Mesoporous Materials*, 60 (1-3):1–17, 2003.

[10] J.M. Hollas. *Moderns Spectroscopy*. Wiley and Sons, Ltd, fourth edition edition, 2004.

[11] Krister Holmberg, Bo Jönsson, Bengt Kronberg, and Björn Lindman. *Surfactants and Polymers in Aqueous Solution*. Wiley and Sons, Ltd, second edition, 2003.

[12] P. Kjellin, H. Ekström, G. Lindbergh, and A.E.C. Palmqvist. On the activity and stability of Sr_3NiPtO_6 and Sr_3CuPtO_6 as electrocatalysts for the oxygen reduction reaction in a polymer electrolyte fuel cell. *Journal of Power Sources*, 168 (2):346–350, 2007.

[13] Freddy Kleitz, Shin Hei Choi, and Ryong Ryoo. Cubic Ia3d large mesoporous silica: synthesis and replication to platinum nanowires, carbon nanorods and carbon nanotubes. *Chemical Communications*, pages 2136–2137, 2003.

[14] P. Lindner and T. Zemb. *Neutron, x-rays and light. Scattering methods applied to soft condensed matter*. Elsevier Science B.V., 2002.

[15] C. Médard, M. Lefèvre, J.P. Dodelet, F. Jaouen, and G. Lindbergh. Oxygen reduction by Fe-based catalysts in PEM fuel cell conditions: Activity and selectivity of the catalysys obtained with two Fe precursors and various carbon supports. *Electrochimica Acta*, 51:3202–3213, 2006.

[16] Sten-Erik Mörtstedt and Gunnar Hellsten. *Data och Diagram*. Liber AB, seventh edition edition, 2003.

[17] Chia-Min Yang, Claudia Weidenthaler, Bernd Spliethoff, Mamatha Mayanna, and Ferdi Schüth. Facile template synthesis of ordered mesoporous carbon with polypyrrole as carbon precursor. *Chemistry of Materials*, 17:355–358, 2005.